

Recent Advances in Grating Coupled Surface Plasmon Resonance Technology

Divagar Murugan, Marcel Tintelott, Madaboosi S. Narayanan, Xuan-Thang Vu, Tetiana Kurkina, César Rodríguez-Emmenegger, Ulrich Schwaneberg, Jakub Dostalek, Sven Ingebrandt, and Vivek Pachauri*

Surface plasmon resonance (SPR) is a key technique in developing sensor platforms for clinical diagnostics, drug discovery, food quality, and environmental monitoring applications. While prism-coupled (Kretschmann) SPR remains a “gold-standard” for laboratory work-flows due to easier fabrication, handling and high through put, other configurations such as grating-coupled SPR (GC-SPR) and wave-guide mode SPR are yet to fulfil their technology potential. This work evaluates the technical aspects influencing the performance of GC-SPR and reviews recent progress in the fabrication of such platforms. In principle, the GC-SPR involves the illumination of the plasmonic metal film with periodic gratings to excite the surface plasmons (SP) via diffraction-based phase matching. The real performance of the GC-SPR is, however, heavily influenced by the topography of the grating structures produced via top-down lithography techniques. This review discusses latest in approaches to achieve consistent plasmonic gratings with uniform features and periodicity over a large scale and explores the choice of plasmon-active and substrate material for enhanced performance. The review also provides insights into the different GC-SPR measurement configurations and highlights on opportunities with their potential applications as biosensors with translational capabilities.

1. Introduction

The phenomenon of surface plasmon resonance (SPR) has consistently drawn attention to study light behavior at the interfaces since 1902 when Wood^[1] observed anomalous patterns of dark and light bands during his experiments with metallic diffraction gratings, which was later interpreted by Rayleigh and Fano. A clear explanation of the phenomenon was, however, given only in 1968 with Otto, Kretschmann, and Raether's elucidating the excitation of surface plasmons (SPs).^[1,2] Later on, Liedberg's demonstrations on utilizing SPR to study biomolecular interactions catapulted the technique further into its use as sensor platforms for the study of chemistry and biology-related topics in molecular science.^[3] SPR continues to attract significant interest from researchers as an established technique to study novel interfaces, biomolecular and cellular interactions.^[4-8]

D. Murugan, M. Tintelott, X.-T. Vu, S. Ingebrandt, V. Pachauri
Institute of Materials in Electrical Engineering 1
RWTH Aachen University
Sommerfeldstrasse 24, 52074 Aachen, Germany
E-mail: pachauri@iwe1.rwth-aachen.de

M. S. Narayanan
Department of Biotechnology, Bhupat and Jyoti Mehta School
of Biosciences
Indian Institute of Technology Madras
Chennai 600036, India

T. Kurkina, U. Schwaneberg
Institute of Biotechnology
RWTH Aachen University
Worringerweg 3, 52074 Aachen, Germany

C. Rodríguez-Emmenegger
DWI-Leibniz Institute for Interactive Materials
Forckenbeckstr. 50, 52074 Aachen, Germany

C. Rodríguez-Emmenegger
Catalan Institution for Research and Advanced Studies (ICREA)
Passeig Lluís Companys 23, Barcelona 08010, Spain

C. Rodríguez-Emmenegger
Institute for Bioengineering of Catalonia (IBEC)
Carrer de Baldiri Reixac, 10, 12, Barcelona 08028, Spain

J. Dostalek
FZU-Institute of Physics
Czech Academy of Sciences
Prague 18221, Czech Republic

J. Dostalek
Laboratory for Life Sciences and Technology (LiST)
Faculty of Medicine and Dentistry
Danube Private University
Krems 3500, Austria

 The ORCID identification number(s) for the author(s) of this article can be found under <https://doi.org/10.1002/adom.202401862>

© 2024 The Author(s). Advanced Optical Materials published by Wiley-VCH GmbH. This is an open access article under the terms of the [Creative Commons Attribution-NonCommercial](https://creativecommons.org/licenses/by-nc/4.0/) License, which permits use, distribution and reproduction in any medium, provided the original work is properly cited and is not used for commercial purposes.

DOI: 10.1002/adom.202401862

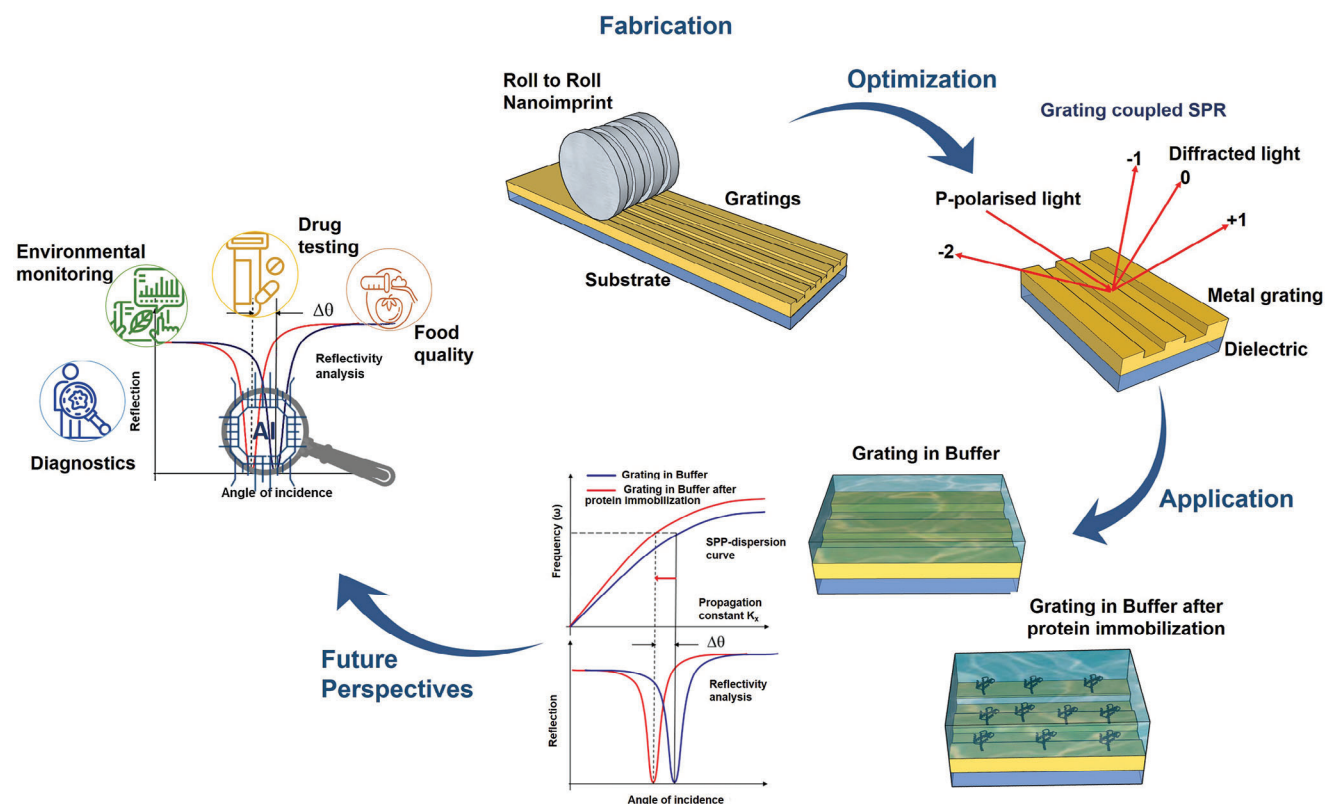


Figure 1. Schematic overview of this review representing the fabrication, measurement configuration, and application of GC-SPR.

In general, plasmonic platforms are realized using noble metals such as gold (Au), and silver (Ag) exhibiting a strong absorption band in visible (Vis) regions of the electromagnetic spectrum, ≈ 520 nm for Au and 380–450 nm for Ag.^[9–12] The SPR condition occurs when the energy carried by the photons incident at a metal–dielectric interface is transferred to the free-electron gas bound to the interface, termed as surface plasmons (SPs). An energy transfer is permitted, when the oscillation frequency of the electron gas at the interface matches the frequency of the incident electromagnetic wave (photons), setting the free-electrons to oscillate against static (positive) charges at the metal surface.^[1,4] Observing SPR using a planar metal surface is nearly impossible due to the propagation constant of surface plasmon being greater than that of the incident light, which does not allow for their phase-matching condition. Therefore, the mismatch between the respective propagation constants is typically circumvented through prism coupling in the Otto configuration and the Kretschmann configurations. In the Kretschmann configuration, the metal layer is illuminated through a high refractive index prism, leading to total internal reflection at the interface and an increase in the propagation constant of the incident light. In comparison to the Otto configuration, the Kretschmann configuration is widely used for biomolecular interaction studies. However, its main disadvantages are low spectral resolution and the requirement of bulky instrumentation.

As an alternative to the Kretschmann and the Otto configuration, grating coupled (GC-SPR) involves light incidence on a

metal film with periodic gratings, while the detector is rotated on an azimuthal axis to obtain high sensitivity.^[13,14] The phase matching conditions in GC-SPR are obtained by a selection of a suitable light wavelength, incidence angle, and grating periodicity, which will be discussed in the following sections of this review. Briefly, the light illuminated on the grating structure gets diffracted into various orders (m); given as 1, -1 , 2, -2 , 3, -3 , etc., and excites SPs, which can be detected as a measure of plasmon resonance.^[15] Plasmon resonances are tuned by varying the topographic features of the gratings such as pitch, amplitude, and shape.^[16–19] The main focus of this review is to serve as a guide with necessary information on the scientific advancement in the field of GC-SPR and its performance. Subsequently, it will delve into the optimization strategies for key features, such as the grating structure, choice of fabrication technology, material composition, and measurement configuration, providing insights into creating a well-tailored GC-SPR system. While offering a comprehensive overview of technological advancements, the review will also focus on the state-of-the-art developments in GC-SPR and the integration of machine learning (ML) techniques as future perspectives in developing a novel GC-SPR (Figure 1).

1.1. Theory of Excitation of Surface Plasmons

In the conventional prism-based Kretschmann configuration, an attenuated total internal reflectance (ATR) is utilized by coating

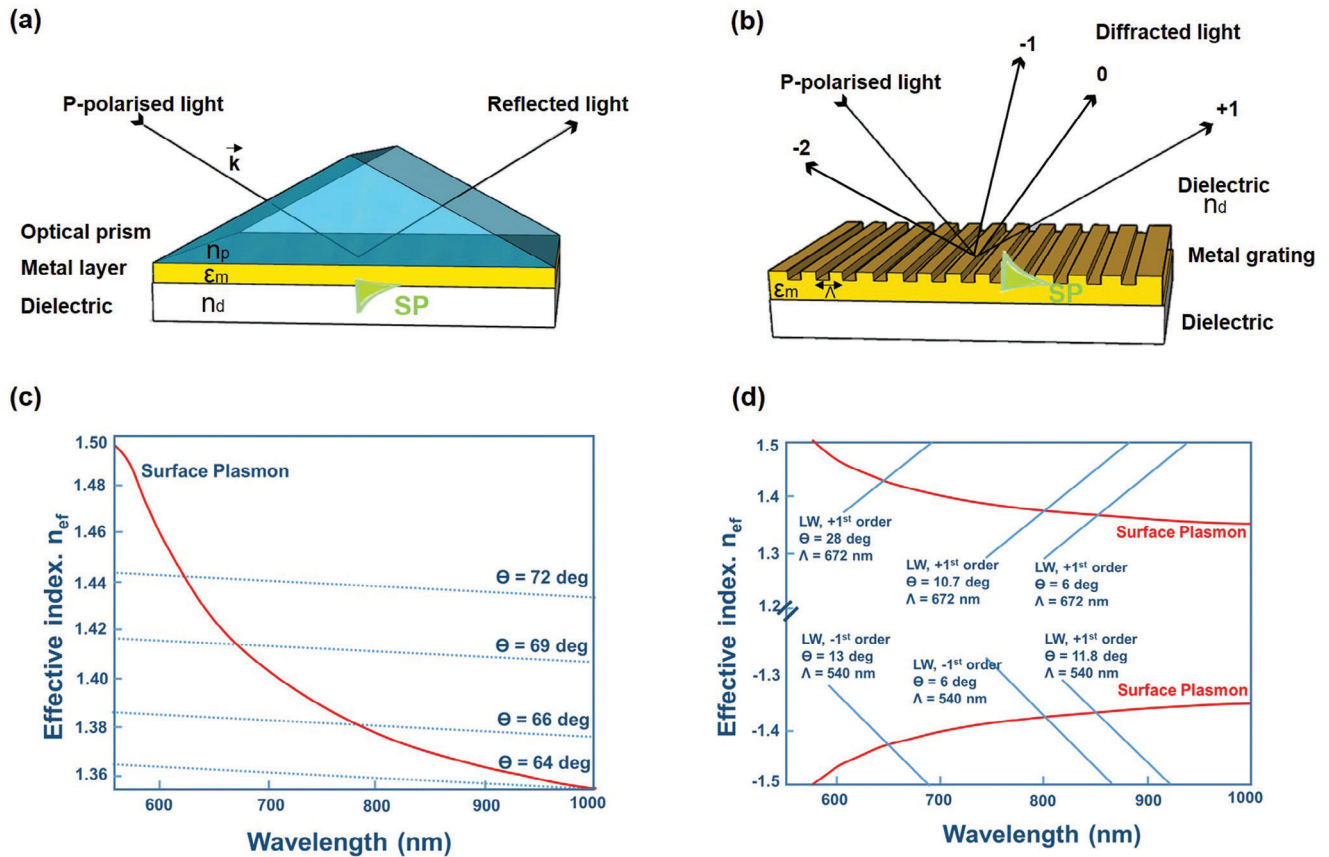


Figure 2. Schematic representation of A) prism and B) grating-coupled SPR. C,D) Spectral dependence of the effective index of surface plasmon (SP) at Au–water interface and evanescent light wave produced using BK-7 glass prism, and D) Spectral dependence of the effective index of the SP at the gold–water interface and light wave produced by two different diffraction gratings ($\Lambda = 540$ nm, and $\Lambda = 672$ nm). It could be noted that the different orders of diffraction can be used to fulfill the matching condition. Figures (C) and (D) were adapted with permission from.[20] Copyright 2006, Springer Nature.

the prism base with a thin metallic film. Briefly, when a light wave propagating in the prism of refractive index (RI) (n_p) is made to fall on a metal film with a semi-infinite dielectric with RI (n_d), a part of the light is reflected back into the prism, and a part penetrates into the metal as a heterogenous inhomogeneous electromagnetic wave, which decays exponentially in the direction perpendicular to the prism-metal interface. This wave is referred to as evanescent. If the metal film thickness (d) is sufficiently thin as less than 100 nm, the evanescent wave reaches the metal film surface and can couple there with SPs. The propagation constant of the surface plasmon (β^{sp}) at the thin metal–dielectric interface (outer boundary) as shown in Figure 2 can be expressed as,

$$\beta^{sp} = \beta^{sp*} + \Delta\beta = \frac{2\pi}{\lambda} \sqrt{\frac{\epsilon_d \epsilon_m}{\epsilon_d + \epsilon_m}} + \Delta\beta \quad (1)$$

where β^{sp*} is the propagation constant of the surface plasmon at the metal–dielectric interface in the absence of the prism, $\Delta\beta$ accounts for the finite thickness (d) of the thin metal film and the presence of prism, ϵ_d , ϵ_m are the permittivity of the dielectric and the metal, respectively. As mentioned earlier for the coupling between the evanescent wave ($\beta^{E.wave}$) and the sur-

face plasmon to occur, the propagation constant of evanescent wave and that of the surface plasmon (β^{sp}) should match. Hence,

$$\frac{2\pi}{\lambda} n_p \sin \theta = k_z = \beta^{E.wave} = \text{Re} \{ \beta^{sp} \} = \text{Re} \left\{ \frac{2\pi}{\lambda} \sqrt{\frac{\epsilon_d \epsilon_m}{\epsilon_d + \epsilon_m}} + \Delta\beta \right\} \quad (2)$$

With reference to Figure 2a, at total internal reflection (TIR) the wave vector k_z in terms of effective index, can be given as

$$n_p \sin \theta = n_{ef}^{E.wave} = n_{ef}^{S.plasmon} = \text{Re} \left\{ \sqrt{\frac{\epsilon_d \epsilon_m}{\epsilon_d + \epsilon_m}} \right\} + \Delta n_{ef}^{S.plasmon} \quad (3)$$

where,

$$\Delta n_{ef}^{S.plasmon} = \text{Re} \left\{ \frac{\Delta\beta \lambda}{2\pi} \right\} \quad (4)$$

$n_{ef}^{E.wave}$ and $n_{ef}^{S.plasmon}$ are the effective indices of the evanescent wave and surface plasmon, respectively. In the coupling conditions are illustrated in Figure 2c, each wavelength has a single satisfying angle of incidence, which increases with decreasing wavelength.

Similarly, in the case of GC-SPR, the light wave is incident on a metal grating, giving rise to a series of diffracted waves that allow for the excitation of the SPs. For instance, assume a metal grating with dielectric constant ϵ_m , grating period Λ , and grating depth of d as shown in Figure 2b. When a light wave with the wavevector k is incident such a metal grating via a dielectric medium with RI of n_d then the wave vector of the diffracted gratings (k_m) can be given as,

$$k_m = k + mG \quad (5)$$

where m denotes the diffraction order, and G is the grating vector, which lies in the plane of the grating vector (plane y - z) and perpendicular to the grooves. Furthermore, the magnitude of the grating vector is inversely proportional to the pitch of the grating and can be expressed as (for the grating geometry considered),

$$G = \frac{2\pi}{\Lambda} z_0 \quad (6)$$

In addition, the component of the wave vector of the diffracted light perpendicular to the plane of the grating k_{zm} is equal to that of the incident light, while it is diffraction altered at the plane k_{zm} . The component of the wave vector at k_{zm} can be expressed as,

$$k_{zm} = k_z + m \frac{2\pi}{\Lambda} \quad (7)$$

This diffracted wave can couple with the SP, if the propagation constant along the grating surface k_{zm} matches with the propagation constant of the SP.

$$\frac{2\pi}{\lambda} n_d \sin \theta + m \frac{2\pi}{\Lambda} = k_{zm} = \pm Re \{ \beta^{sp} \} \quad (8)$$

where,

$$\beta^{sp} = \beta^{sp*} + \Delta\beta = \frac{2\pi}{\lambda} \sqrt{\frac{\epsilon_d \epsilon_m}{\epsilon_d + \epsilon_m}} + \Delta\beta \quad (9)$$

In which, β^{sp*} denotes the propagation constant of the surface plasmon propagating along the smooth interface of a semi-finite metal and a semi-finite dielectric, and $\Delta\beta$ accounts for the presence of gratings. In terms of effective index, the coupling condition can be rewritten as,

$$n_d \sin \theta + m \frac{\lambda}{\Lambda} = \pm \left(Re \left\{ \sqrt{\frac{\epsilon_d \epsilon_m}{\epsilon_d + \epsilon_m}} \right\} + \Delta n_{ef}^{S, plasmon} \right) \quad (10)$$

where, $\Delta n_{ef}^{S, plasmon} = Re \left\{ \frac{\Delta\beta \lambda}{2\pi} \right\}$. Figure 2d, shows the coupling condition between a diffracted wave and a surface plasmon. It can be noted that the matching condition is fulfilled by different orders of diffraction for a given grating pitch. The coupling condition can be fulfilled for various combinations of the angle of incidence, grating pitch, and diffraction order. Furthermore, it can be noted that for a positive diffraction order, the coupling wavelength increases with a decreasing angle of incidence and vice versa for negative diffraction orders.

2. Measurement Configuration for GC-SPR

In this section, we will provide an overview of different read-out methods and setups, which have been used for GC-SPR. We will describe measurement setups for angle, wavelength, and phase/polarization interrogation, as shown in Figure 3,

2.1. Angular Interrogation

Angular interrogation is the most widely explored measurement configuration of SPR and GC-SPR. Angular interrogation in GC-SPR involves varying the angle of incident light to study changes in the resonance condition, providing insights into the biomolecular interaction at the grating-dielectric (sensing medium) interface. Angular interrogation systems are sensitive to the local RI changes at the interface, which is studied by plotting the reflected light intensity as a function of varying incident angles. Typically, this type of measurement configuration measures the angle at which the greatest loss of reflected light occurs, which is known as SPR minimum. Later, the sensitivity is measured in terms of angle shift per RI unit ($^\circ$ /RIU) by considering the angles of SPR minimum corresponding to each RI. An angle interrogation setup to measure the response of a GC-SPR chip consists of a laser, an optical chopper, a polarizer, a motorized stage for controlling the incident angle, a photodiode, and a lock-in amplifier, as shown in Figure 3a. For instance, a He-Ne laser (632.8 nm wavelength) is directed on a sample, and the light passes an optical chopper (reference signal for the lock-in amplifier) and two polarizers for polarization and intensity control. The reflected light at the GC-SPR chip surface (any order of choice depending on the experimental design) is monitored by a photodiode (lock-in technique) while measuring at different angles.

2.2. Wavelength Interrogation

In the wavelength interrogation configuration, the sample is illuminated with a broad-band light source, and the wavelength of the reflected light is scanned using a spectrometer at a fixed angle, as shown in Figure 3b. The effective RI at the grating-dielectric interface alters the resonance matching condition, leading to the shift in the SPR minimum to higher wavelengths. The sensitivity of wavelength interrogation systems is studied by plotting the intensity of reflected light as a function of wavelength, which is expressed in terms of wavelength shift per RIU (nm RIU^{-1}). For example, Dou and co-workers utilized an experimental configuration consisting of a $2 \times 2 \text{ cm}^2$ DVD piece coated with Au, a 2 mm thick polydimethylsiloxane spacer, and a micro glass slide as a grating coupler.^[21] The experimental setup consists of a halogen light source, a high-resolution spectrometer (HR4000 and NIRQuest512 Ocean Optics), and a reflection probe (R600-7) to monitor the SPR resonance. Briefly, the light from the halogen light source initially passes through a collimated convex lens, followed by the Glan-Taylor polarizer, and hits the grating coupler at an oblique angle (can be tuned). A fiberoptic spectrometer captures the reflected light

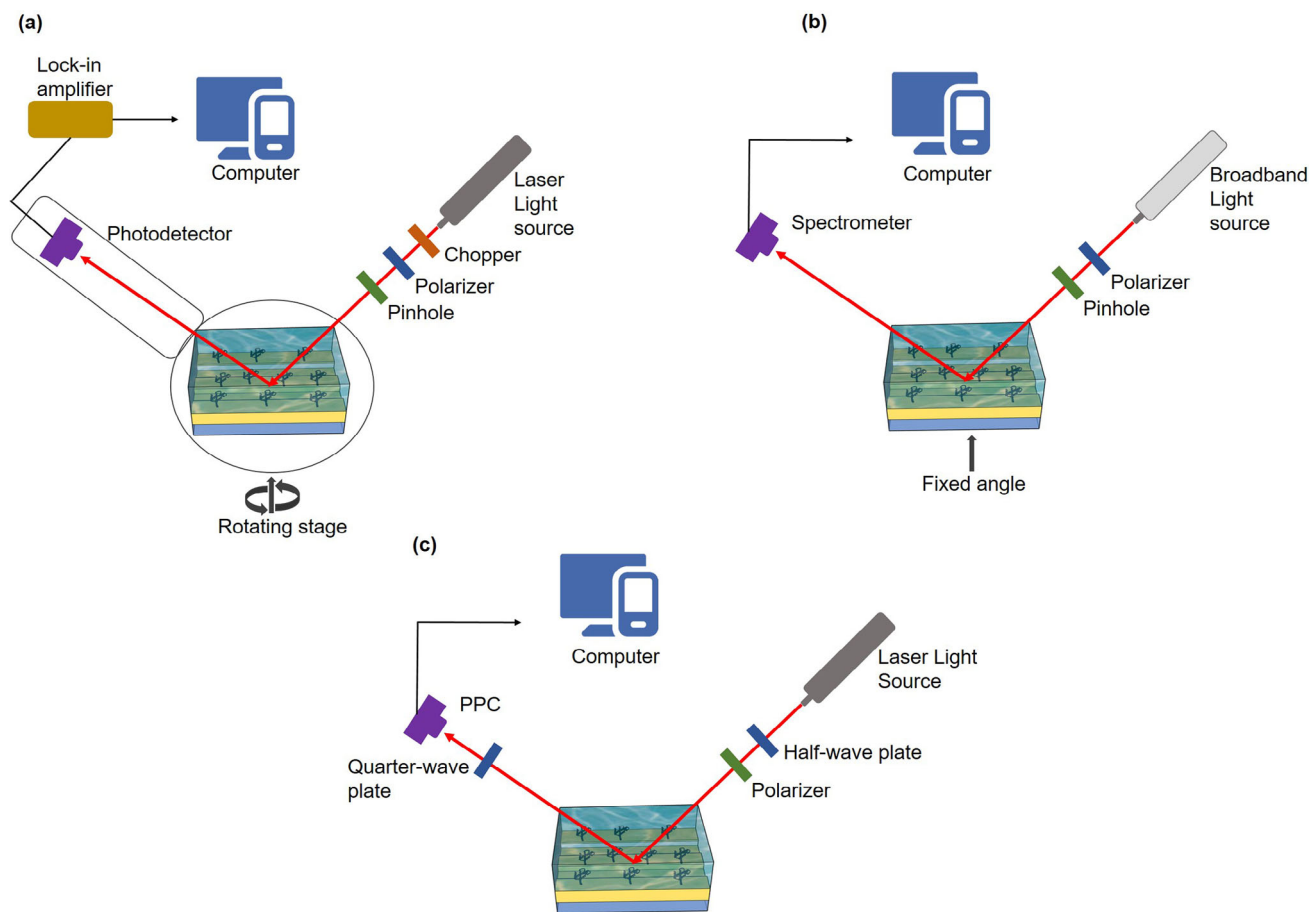


Figure 3. Simple schematic representation of three different readout configurations of GC-SPR: a) angular interrogation, b) wavelength interrogation, and c) phase/polarization interrogation.

from the grating coupler and the sensitivity had been found to be $961.5 \text{ nm RIU}^{-1}$ with FOM of 60.^[21] Similarly, Saito and co-workers presented a wavelength interrogation-based measurement configuration. They used a supercontinuum light source. Here, a single wavelength light was obtained using an acousto-optical tunable filter unit (Fianium, NIR2, U.K.). The light passed through a polarizer and a long pass filter ($\lambda > 1000 \text{ nm}$). To measure the irradiating light and the reflected light a half mirror was used. The intensities were measured using power meters.^[22]

2.3. Phase/Polarization Interrogation

Phase/polarization interrogation relies on the measurement of the phase of the light or its polarization state upon interaction with a sensor surface.^[23] This technique can provide additional details information about the grating-dielectric (sensing medium) interface leading to enhanced sensitivity and specificity in detecting biomolecular interactions. In general, the phase of the light is altered when it interacts with the SPPs at the grating-dielectric interface, which is sensitive to the RI changes. Furthermore, the polarization dependency of the SPR

can also be monitored by the biomolecular interactions at the grating-dielectric interface. Usually, SPPs are excited preferably by p-polarized light, while the s-polarized light is insensitive. Hence, by comparing the phase shift of p- and s-polarized light, one can monitor the changes at the grating-dielectric interface. The phase shift of the reflected light can be expressed as follows,

$$\vartheta = \arctan \left(\frac{\Delta k}{\Gamma} \right) \quad (11)$$

where, Δk is the momentum mismatch between the SPP and the diffracted light, and Γ is the damping factor, which includes both intrinsic and radiative losses.

However, the phase-sensitive GC-SPR is less explored due to the complex optical instrumentation and limited dynamic range. In general, the experimental setup consists of an incident light source that crosses a half-wave beam splitter mounted on a rotating stage. The laser beam passing the half-wave beam splitter illuminates the grating structure based on a rotational stage to select the azimuthal angle and the reflected light from the sample gratings is captured using a CMOS camera, as shown in Figure 3c. The laser beam and the CMOS detector were

Table 1. Overview of different measurement configurations and their corresponding sensitivity.

Light source	Method	Detector	Sensitivity	Refs.
Laser 635 nm	Phase interrogation	Photodetector array (Hamamatsu S4111, 16 elements)	193.5 deg RIU ⁻¹	[25]
Laser beam at 633 nm	Phase interrogation	CMOS camera	100 cells mm ⁻²	[26]
White light halogen	Wavelength interrogation	Spectrometer	Reference channel – 321.78 nm RIU ⁻¹ Test channel – 514 nm RIU ⁻¹	[27]
He–Ne laser (wavelength 632.8 nm)	Angular interrogation	CCD detector	160 deg RIU ⁻¹	[18]
Tungsten halogen light source (LS-1)	Wavelength interrogation	High-resolution spectrometers, (HR4000 and NIRQuest512, both from Ocean Optics)	858 nm RIU ⁻¹	[21]
Light beam (635 nm-wavelength)	Phase polarization	CMOS camera	–	[28]
Supercontinuum light source	Wavelength interrogation	Power meter	–	[22]
Deuterium-halogen lamp	Wavelength interrogation	Spectrometer	2077.26 nm RIU ⁻¹	[29]
Laser	Phase-interrogation	CMOS camera	–	[24]
He–Ne laser	Angle-interrogation	Photo diode	–	[30]
He–Ne laser	Angle-interrogation	PMT	–	[31]
Laser Diode	Angle-interrogation	PMT/CCD camera	–	[31]
Smartphone LED	Wavelength interrogation	CMOS camera (smartphone)	–	[32]
He–Ne laser	Angle-interrogation	Photodiode coupled to a lock-in amplifier	–	[33]
Halogen lamp	Wavelength interrogation	Imaging spectrometer equipped with a CCD camera	687 nm RIU ⁻¹	[34]
White light source	Wavelength interrogation	Fiber optic spectrometer	–	[35]
Unpolarized light	Wavelength interrogation	Spectrophotometer	210 nm RIU ⁻¹	[36]
Deuterium-halogen lamp	Angle-interrogation	Fiber optic spectrometer	961.5 nm RIU ⁻¹	[37]
Laser diode	Angle-interrogation	CCD camera	95 deg RIU ⁻¹	[38]
Super luminescent diode	Wavelength interrogation	Spectrometer	285 nm RIU ⁻¹	[39]

attached to the articulated base to facilitate a polar angle rotation. For example, Sonato and co-workers in 2016, utilized a detection setup for phase-interrogation SPR consisting of a laser (635 nm wavelength; Thorlabs, Inc.; <5.0 mW of output power; class 3R), a polarizer (Thorlabs, Inc.: LPVISE100-A), a sample holder (Edmund: 56–794, Thorlabs, Inc.: DT25/M), and a CMOS camera (Thorlabs, Inc.: DCC1545M). Here, an incident light beam with a wavelength of 635 nm passed through a polarizer and rotating half-wave beam splitter reaching the GC-SPR chip mounted on a rotation stage (Edmund: NT55-028). The reflected light is then collected using a CMOS camera for detection.^[24] The following **Table 1**, compares the performance metrics of each of the measurement configurations reported in the literature, followed by **Table 2**, which comprehensively compares the key features of these measurement configurations.

3. Grating Structure and Its Influence on the Performance of GC-SPR

In this section, the significance of the grating structures, especially the sinusoidal gratings and the rectangular gratings in determining the sensitivity of the GC-SPR will be discussed in detail.

3.1. Sinusoidal Grating Structure

Sinusoidal gratings shown in **Figure 4a** are the most common grating structures explored for the development of GC-SPR.^[40–42] Within the sinusoidal gratings, several features, including periodicity, grating depth, and grating thickness can largely influence the overall sensitivity. For instance, in the year 2016 Wei Su, reported the optimization of sinusoidal grating constant, grating thickness, and substrate thickness through numerical simulations for silver (Ag) and gold (Au) gratings.^[41] It has been reported that Ag sinusoidal gratings with optimized features of periodicity (Λ) = 800 nm, pitch depth (d) = 50 nm, and $h = 40$ nm have a sensitivity of 193.9° RIU⁻¹, while Au gratings have 186.9° RIU⁻¹. Apart from the angular interrogation, Wang and his co-workers in 2020 reported a wavelength-based interrogation using Ag sinusoidal structure on a silicon substrate with a periodicity (Λ) of 1120 nm and a depth of 18 nm obtained through a nanosecond laser interference lithography. The sensitivity of the fabricated sinusoidal gratings has been found to be 961.5 nm RIU⁻¹.^[37] It can be noted that these reports involve different periodicity within the sinusoidal gratings, however direct correlation to determine the optimal periodicity is challenging due to the difference in the interrogation schemes. Interestingly, Long et al. in 2020, reported such a comparison, studying the influence

Table 2. Comparison of different measurement configurations.

Parameter	Angular interrogation	Wavelength interrogation	Phase polarization
Sensitivity	High	Moderate	Excellent
Dynamic range	Wide	Limited	limited
Measurement speed	Slow (due to mechanical scanning)	Fast	Super-fast
Setup complexity	Moderate	Low	High
Miniaturization potential	Low	High	Low
Mechanical stability	Sensitive to vibrations	Stable	Highly sensitive to disturbances
Light source requirements	Monochromatic	Broadband	Monochromatic with precise polarization control
Detector requirements	Photodiode	Spectrometer	Phase-sensitive detectors
Multiplexing capability	Limited	High	Moderate
Realtime monitoring	Limited by scanning speed	High	Excellent
Portability	Low	High	Low
Cost	Moderate	Low	High
Single-molecule detection	Challenging	Highly-challenging	Possible
Key advantages	Well-established process with good overall performance	Compact and suitable for portable devices	High sensitivity for detection at lower limits
Key disadvantages	Movable components, bulky and slower measurement rate	Relatively lower sensitivity	Complex setup and sensitive to the disturbances

of the periodicity of the sinusoidal gratings on the sensitivity of the GC-SPR. Accordingly, the sensitivity of the sinusoidal grating structures with varying periodicity, including 314, 1470, and 6733 nm have been found to be 319.96, 1477.74, and 2077.26 nm RIU⁻¹,^[40] respectively. However, it is important to note that gratings with 314 nm periodicity have been made using Ag, while the other two grating structures were made using aluminum (Al). Nevertheless, from these reports, it could be clearly seen that the increase in periodicity leads to enhanced sensitivity. Similarly, the same article also suggests that lower depth leads to higher sensitivity through theoretical and experimental validations. Briefly, considering the period as 560 nm and the thickness of Ag film as 100 nm, the grating depth has been varied from 10 to 120 nm.^[40] It has been found that the depth of the period significantly affects the reflectivity minimum and the FWHM of the SPR peak due to the change in the propagation constant of the diffracted light. The propagation constant decreases with an increase in the periodicity depth, which in turn broadens the SPR peak and reduces the reflectivity. Hence, a compromise must be established in determining the periodicity depth that exhibits narrow Full-width half

maxima (FWHM) with minimum reflectivity. It is also important to note that there exists a lower limit for the depth below which the sensitivity decreases due to a drastic increase in the FWHM of the SPR peak.^[43–46]

Besides continuous sinusoidal grating structures with defined pitch and periodicity, researchers have also explored sinusoidal-like periodic structures such as DVD grooves. For instance, Dou and his co-workers compared a plane DVD disc and a movie DVD disc.^[21] The track pitch of the plane DVD has been characterized to be ≈740 nm, while the movie DVD has the same track pitch with randomly arranged short and long pits. The sensitivities of the plane and the movie DVD discs through wavelength scan have been found to be 858 and 645 nm RIU⁻¹, respectively. The results obtained had also been validated using numerical simulation through a Lumerical finite-difference time-domain (FDTD) algorithm with input parameters including track pitch of 740 nm, track width of 500 nm, track sidewall tilting angle of 80°, and groove depth of 100 nm.^[21] From the results presented, it can be noted that the RI sensitivity increases with the continuous topography of the periodic structure, which has

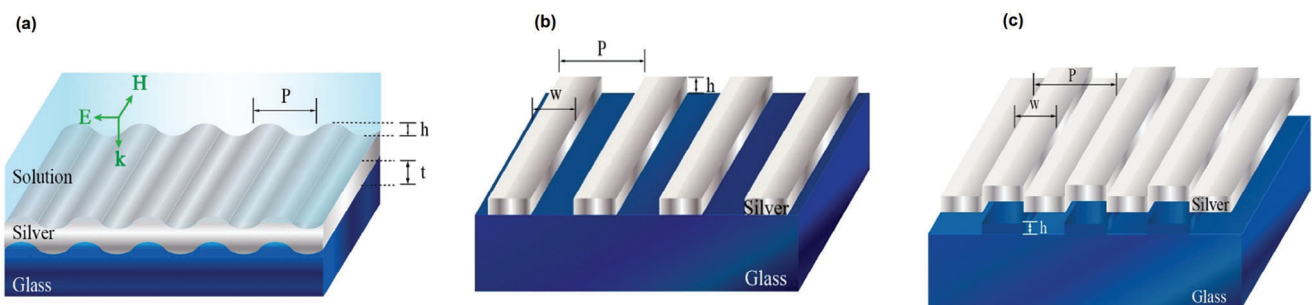


Figure 4. General representation of different grating topologies including sinusoidal a), discontinuous rectangular b), and continuous rectangular c). Reproduced with permission from.^[40] Copyright 2020, Elsevier.

been attributed to the boundary conditions and plasmon coupling of the propagating SPs. Furthermore, plasmon coupling on the movie disc with long and short pits has been evidenced with two resonance peaks originating due to the inter-pit interaction of plasmons between the data tracks and along the data tracks.

In summary, the investigation into sinusoidal grating structures for GC-SPR applications has revealed a wealth of insights into the factors influencing sensitivity. The optimization of periodicity, grating depth, and thickness plays a pivotal role in determining the overall performance. Notably, the studies aforementioned have demonstrated the impact of varying these parameters on sensitivity, with different materials and periodicities yielding diverse outcomes. Especially Long et al.'s comprehensive comparison of sinusoidal grating structures with varying periodicities highlighted the correlation between increased periodicity and enhanced sensitivity.^[40,47–50] Furthermore, the depth of the periods has been shown to influence reflectivity and FWHM of the SPR peak, emphasizing the need for a careful compromise to achieve optimal performance. Beyond continuous sinusoidal structures, researchers have delved into discontinuous structures, exploration of DVD discs outlays the significance of continuous topography in maximizing sensitivity, attributed to boundary conditions and plasmon coupling. Overall, optimizing the structural parameters in sinusoidal gratings provides a foundation for tailoring GC-SPR platforms to specific applications.

3.2. Rectangular Grating Structures

In addition to the sinusoidal gratings, researchers have also utilized continuous and discontinuous rectangular grating structures to realize a GC-SPR, as shown in Figure 4b,c. The rectangular gratings are typically fabricated on a plasmonic thin film and are designed as self-referenced SPR.^[28,51–54] The discontinuous rectangular gratings fabricated on a plasmonic thin-film give rise to two SPR dips due to the presence of two interfaces, one between the plasmonic metal and the grating metal and the other one between the grating metal and the surrounding medium. In 2015, Abutoma and his co-workers reported the use of silicon nitride (Si_3N_4) grating structures on top of an Ag film to realize a self-referenced SPR.^[51] The reported grating structure had a periodicity of 1000 nm, a width of 550 nm, and a height of 175 nm. The grating structure mentioned above had a sensitivity of $\approx 580 \text{ nm RIU}^{-1}$. Similarly, Anuj et al., in 2019 reported the use of rectangular titanium oxide (TiO_2) grating structures on an Au-film to demonstrate a sensitive GC-SPR.^[52] The reported work also studied the influence of the RI of the substrate material on the overall sensitivity while optimizing the structure parameters, which will be discussed later in the sections on the substrate material. The optimal grating features on a silicon oxide substrate have been found with a periodicity of 980 nm, a width of 500 nm, and a height of 135 nm on an Au-film of thickness of 50 nm. The optimized parameters have been shown to generate a sensitivity of $696.66 \text{ nm RIU}^{-1}$. Among these reported structures, it is difficult to comment on the influence of the grating features on the sensitivity as they involve too many variants, including the materials used to create the grating structures, the

plasmonic thin layer used, their thickness, the interface characteristics of the grating and plasmonic material, and the grating parameters. Generally, rectangular gratings are less explored for establishing GC-SPR due to challenges in the fabrication processes.

3.3. Sinusoidal Gratings Versus Rectangular Gratings

Recently, in 2020, Long et al. systematically compared the sensitivity of a sinusoidal grating with a continuous Ag film and rectangular grating with and without a continuous Ag film. In order to have an efficient comparison, a parameter termed figure of merit (FOM^*) has been defined, which combines sensitivity, FWHM, and depth of the SPR absorption peak.^[40] In general, the FOM combines the sensitivity (S) and FWHM of the SPR absorption peak, $\text{FOM} = S/\text{FWHM}$. However, in order to nullify the effect of noise due to shallow peaks, the FOM was modified considering the absorption peak depth, given as $\text{FOM}^* = \text{Absorption peak depth} \times S/\text{FWHM}$. Particularly, this study included the optimization of various parameters such as grating period, metal film thickness, and duty cycle to optimize the sensitivity of GC-SPR. In addition to the experimental data, simulations have also been carried out using Lumerical FDTD. First, it has been reported that the sensitivity of the GC-SPR is directly proportional to the grating period, which is similar to the findings with the sinusoidal grating structures.

Furthermore, it is interesting to note that the discontinuous Ag film with a depth of 40 nm and a duty cycle of 0.5 generates three peaks in the reflection spectra. Among these three peaks, the electric field analysis shows that two peaks are due to SPRs at the solution-metal interface, and the third peak is due to SPR at the glass-metal interface. It has also been shown that the SPR peaks are asymmetric as opposed to the SPR peaks of the continuous films. Further studies have shown a duty cycle of 0.8 and a grating depth of 24 nm being optimum for the rectangular grating with discontinuous Ag film giving rise to a sensitivity of $556.40 \text{ nm RIU}^{-1}$, while the FOM^* had been reported as 25.23. While the sinusoidal grating and rectangular gratings with continuous Ag film have been shown to exhibit a sensitivity of $\approx 574.56 \text{ nm RIU}^{-1}$ ($\text{FOM}^* = 99.25$) and $568.46 \text{ nm RIU}^{-1}$ ($\text{FOM}^* = 123.70$), respectively. Thus, the results show that in the case of rectangular gratings continuous structures perform better than discontinuous grating structures, while sinusoidal gratings outperform both. The lack of sensitivity with the discontinuous rectangular gratings could be attributed to the coupling of light at the backside of the metal gratings and the SPR modes being affected by plasmon coupling, which is also observed in the movie discs with discontinuous topography as discussed earlier.

3.4. Irregular Structure-Based GC-SPR

In addition to the regular sinusoidal or rectangular grating structures, researchers have also explored irregular patterns in realizing a GC-SPR. For instance, Yeh et al. reported the use of a chirped diffraction grating on poly(dimethoxysilane) (PDMS)

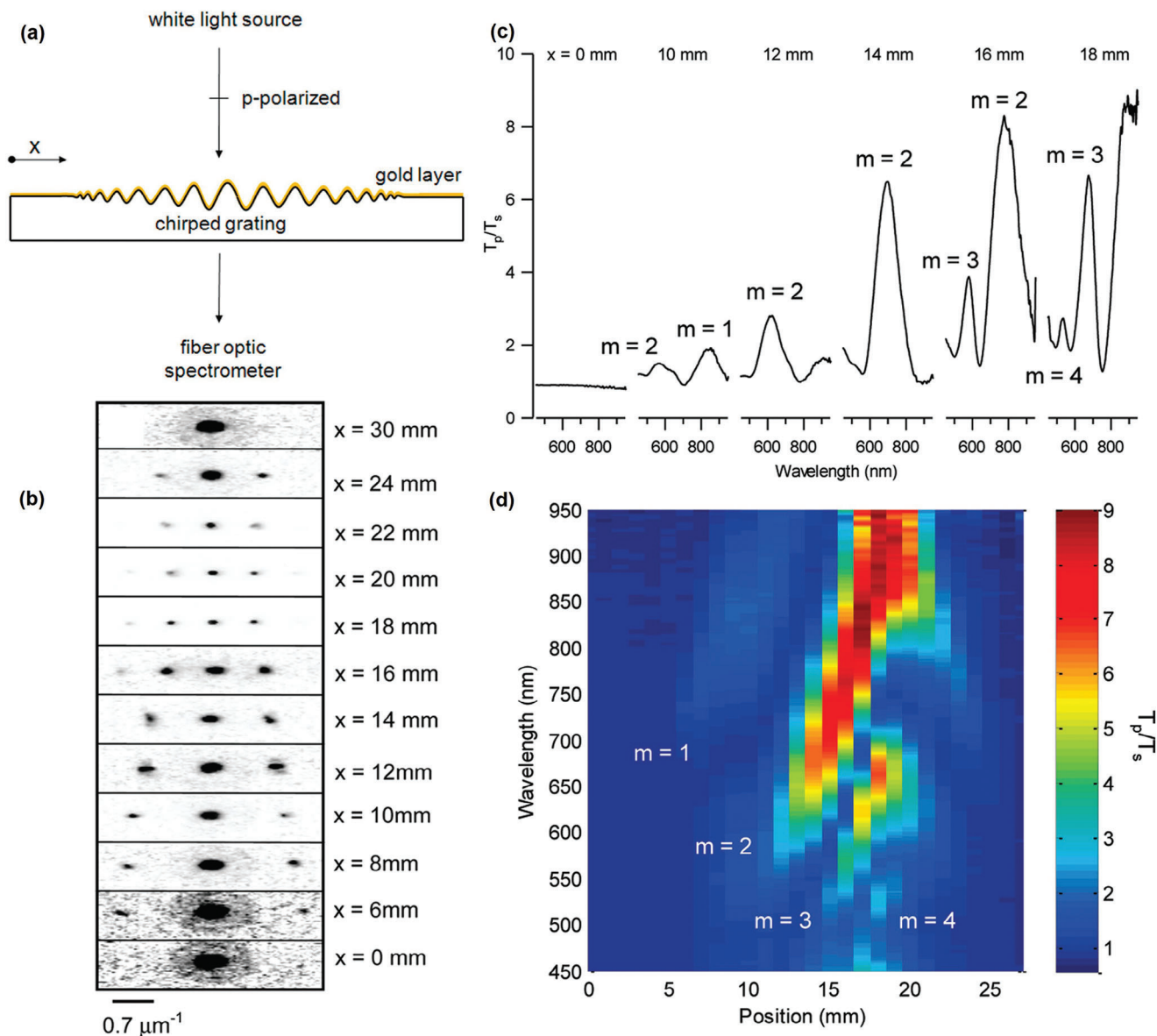


Figure 5. a) Schematic of chirped diffraction gratings and the optical measurement configuration. b) Optical diffraction images (inverted contrast) acquired from the transmission of 630 nm of light at various x-positions along the center of the diffraction grating. c) Selection of transmission spectra (T_p/T_s , ratio of transmitted p-polarized light to s-polarized light) as a function of x-position along the center of the gold-coated diffraction grating. d) Compilation image of transmission spectra (T_p/T_s) acquired every 1 mm between $x = 0$ and $x = 19$ mm along the center of the gold-coated diffraction grating. The diffraction order (m) associated with each transmission peak is noted in the figures. Reproduced with permission from.^[35] Copyright 2010, American Chemical Society.

with spatial variation in both pitch and amplitude along its surface.^[35] The chirped pattern is anticipated to provide varying surface plasmon coupling along the surface of the sample, which has been characterized by measuring the ratio of transmitted p and s polarized light, which is of the nominal value of 1 without gratings. The chirped diffraction grating has been well characterized using the Fourier spectrum of the sample images on the microscopic imaging plane. It has been shown that the grating pitch and amplitude (buckling) are high at the center and decrease at the corners (Figure 5). The AFM studies have shown a profile of grating structure on the PDMS replica with an Au

film of 40 nm, as a function of x-position. Initial buckling has been noticed at $x = 5$ mm with an amplitude < 15 nm and a pitch of ≈ 600 nm. While the pitch maxima of ≈ 1475 nm and amplitude of 245 nm have been observed at $x = 19$ mm, a further increase in x had been characterized to have a decrease in pitch and amplitude until $x = 25$ mm and then there exists a smooth surface.

It has also been shown that the spacing between the diffraction spots is inversely proportional to the pitch value of the grating structure. A minimum spacing of first-order diffraction of $\approx 0.75 \mu\text{m}^{-1}$ has been achieved, corresponding to a pitch value

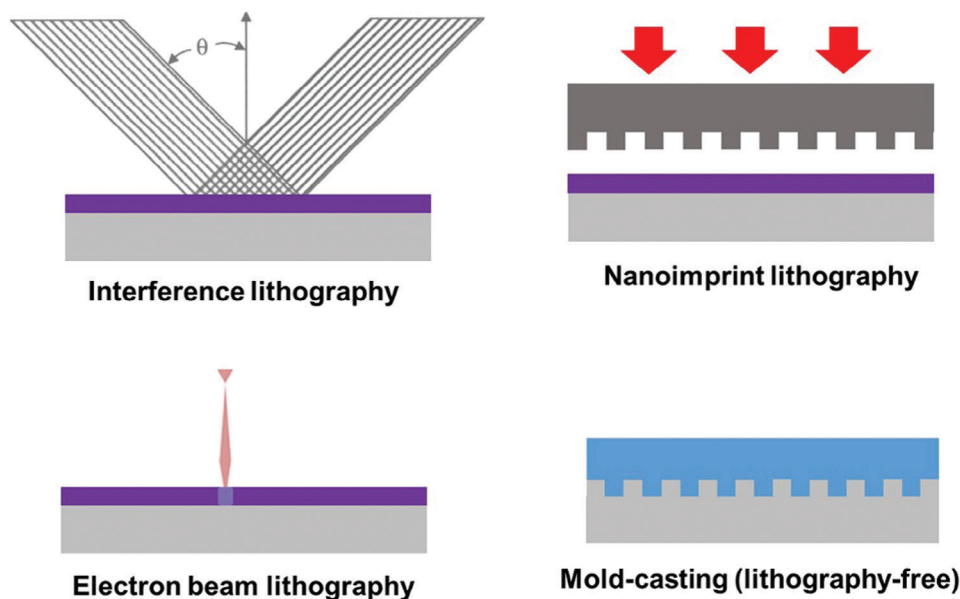


Figure 6. Different fabrication methods are described in the state-of-the-art literature. Lithography-based approaches such as laser interference lithography, nanoimprint, electron beam lithography, and DVD/CD-based mold casting are reported to realize GC-SPR sensor chips.

of 1450 nm at the center. Furthermore, through optical characterization, it has been shown that the pitch value governs the momentum-matching conditions. For instance, at $x = 10$ nm, where the pitch is ≈ 810 nm, two peaks had been observed at ≈ 850 and ≈ 550 nm, which corresponds to the first and second-order scattering, respectively. Further, as the pitch increases, authors have observed a red shift and an enhanced magnitude in the resonance. Another order seemed to originate as the x further increased, the third diffraction order was observed at $x = 16$ nm, and the fourth diffraction order was observed at $x = 18$ nm. Despite the presence of various orders, it has been found that the second-order diffraction has been pronounced in all x values. However, the $m = 1$ was not characterized as it moved away from the sensitive region of the spectrometer used. After the optical characterization, the sensitivity of the chirped grating structure was evaluated by coating a thin layer of SiO_2 . The coating studies have shown that the coating of SiO_2 leads to a clear redshift in all four diffracted angles. The highest sensitivity had been seen with the lowest diffracted angle for a given pitch value. This exploration of irregular patterns expands the design space of GC-SPR platforms, opening new avenues for innovative sensing applications and advancement in plasmonic sensing platforms. Integration of modern machine learning (ML) algorithms and multiplexing may enhance the versatility of these novel plasmonic sensing platforms.

4. Fabrication of Grating-Coupled SPR Platforms

As seen in the previous section, GC-SPR chips can be realized with differently shaped grating structures, different materials, and hence, process flows. Apart from the irregular structures, the fabrication of conventional sinusoidal or rectangular structured surfaces is straightforward by utilizing the standard cleanroom processes or alternative cleanroom-free process flows.

The following section summarizes various fabrication methods (Figure 6) utilized to generate different grating structures.

4.1. Interference Lithography-Based Approach

In the field of nanofabrication techniques, interference lithography stands as a powerful and sophisticated method for patterning structures with dimensions at the nanoscale. This approach utilizes the interference of multiple coherent light waves to create intricate and well-defined patterns. Interference lithography has gained prominence in various fields, including optics, electronics, and particularly in the development of advanced GC-SPR sensor chips. Its ability to achieve high-resolution patterning makes it a valuable tool for creating periodic structures, such as gratings, essential for guiding and manipulating SPR. In the subsequent discussion, we delve into the utilization of interference lithography as a pivotal element in the fabrication of GC-SPR chips on transparent glass substrates.

Transparent glass substrates are widely used for the fabrication of SPR and GC-SPR sensor chips.^[55,56] In the following, several approaches to fabricating rectangular-shaped GC-SPR chips using glass substrates will be discussed in detail. For instance, a GC-SPR chip can be realized by a relatively simple metal lift-off approach. Briefly, it could be a two-step process of evaporating a metallic bilayer (5 nm Cr + 40 nm Au) on a glass substrate, followed by a laser interference lithography-based lift-off process of a second 40 nm Au layer.^[26,28] Gazzola et al., 2016 reported such as process, wherein the first step, chromium (Cr) (5 nm) and Au (40 nm) metal stack had been deposited by electron beam evaporation onto a 25×25 mm² microscope glass slide (Figure 7). After the metal deposition, the sample was coated with S1805 (MICROPOSIT) diluted in propylene glycol monomethyl ether

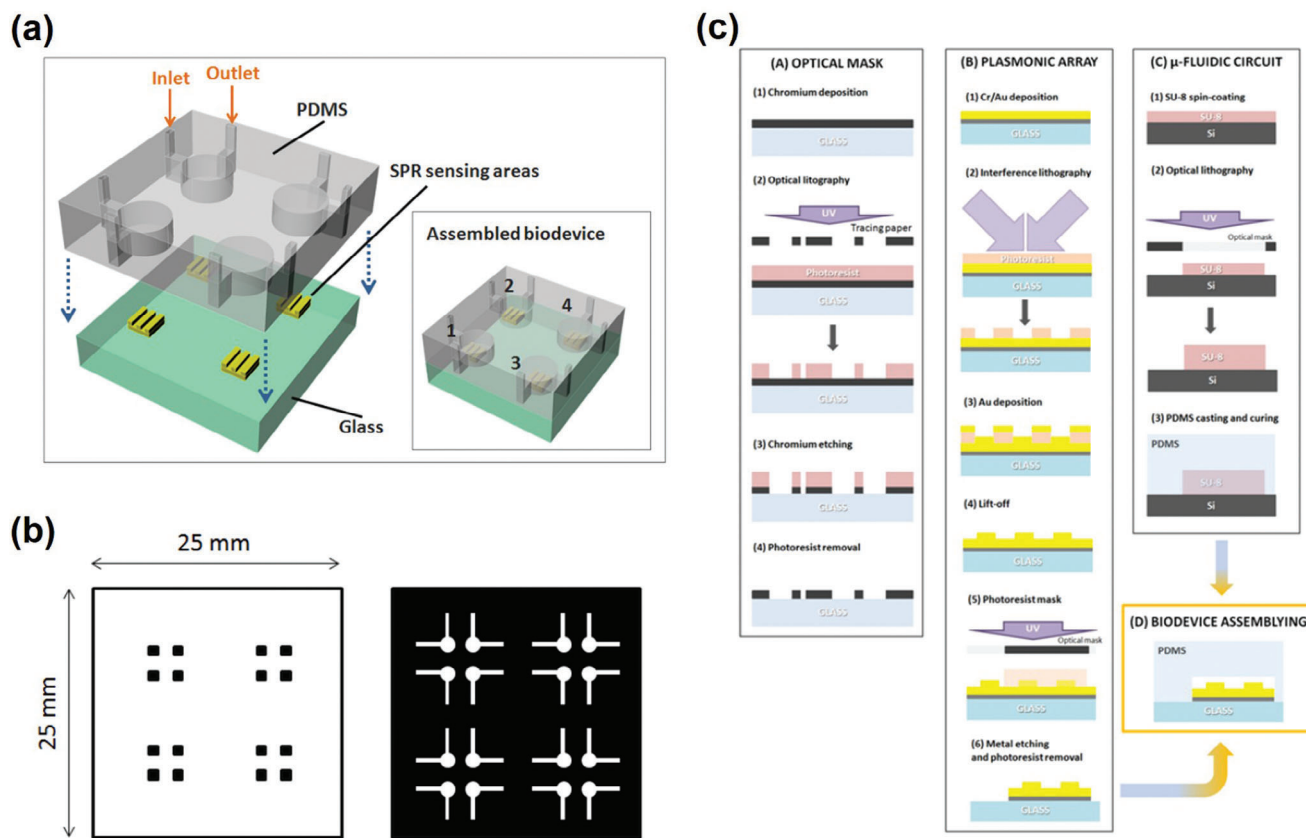


Figure 7. A) Schematic representation of sensor chip with plasmonic gratings supported onto a glass substrate and covered by a PDMS microfluidic compartment. B) Optical masks design to aid the pattern of four biochips in a single exposure and corresponding four circuits with a channel thickness of 200 μm and a cell diameter of 1.5 mm. C) The steps involved in the fabrication of optical masks and the sensor substrates. Reproduced with permission from.^[28] Copyright 2016, E. Gazzola et al.

acetate (PGMEA) (Microresist Technology) in a ratio of 2:3. The resist has been patterned by laser interference lithography and developed in MF-321 (MICROPOSIT). Subsequently, a 40 nm Au layer was deposited on the patterned sample. Finally, the grating structure has been realized by a lift-off process in acetone (at 65 $^{\circ}\text{C}$). Furthermore, versatility in creating complex sensing spots had been demonstrated using an additional UV lithography process, in combination with a metal etching step to create a 4×4 sensing spot array. In the end, in order to enable the addressability of each sensing spot, a microfluidic compartment was utilized using a standard optical lithography process with spin-coated SU-8 resist on a silicon substrate. Later, the structure was used for the casting of a PDMS film to create a fluidic flow cell. The fluidic flow cell has been bonded to the plasmonic sensor chip using a 2-step oxygen/argon plasma treatment. The process outlined provides complete insight into developing a functional GC-SPR platform for a diverse practical application. Further developments could be incorporated in terms of exploring alternative materials for increased sensitivity and advanced surface modification techniques toward tailored biosensing applications. As the field continues to evolve, the integration of interference lithography with a novel fabrication process could result in innovative GC-SPR platforms.

4.2. Nanoimprint-Based Approach

The classical nanoimprint lithography (NIL) process utilizes a mold-to-like structure, called a NIL resist to generate the desired structure on a substrate. Such molds are typically fabricated using silicon or glass substrates. In addition, polymers such as PDMS replications can also be used for this purpose.^[32,57,58] For instance, Wang et al., 2012 utilized the NIL process to develop a sensitive GC-SPR platform to detect bacterial pathogens through magnetic nanoparticle assay.^[58] Briefly, a silicon master with a sinusoidal structure was fabricated using interference lithography and reactive ion beam etching. The silicon master had been utilized to cast PDMS stamps, which have been used to transfer the grating structures onto the plasmonic sensor platform. In order to transfer the structures, a 100 nm Au layer was sputter deposited on a flat glass substrate and coated with a low-RI fluoropolymer film. A NIL process was used to realize the grating structures in the Cytop polymer layer using the PDMS stamp. After the NIL process, a second metal layer (Au) has been deposited using sputtering to finalize the grating coupled SPR chips.^[18]

Similarly, in 2008–2009, Zhang, Hong, and Knoll reported a disposable polymeric sensor chip combined with microfluidic channels. In this work, poly-ethylene-co-acrylic acid (PEAA)

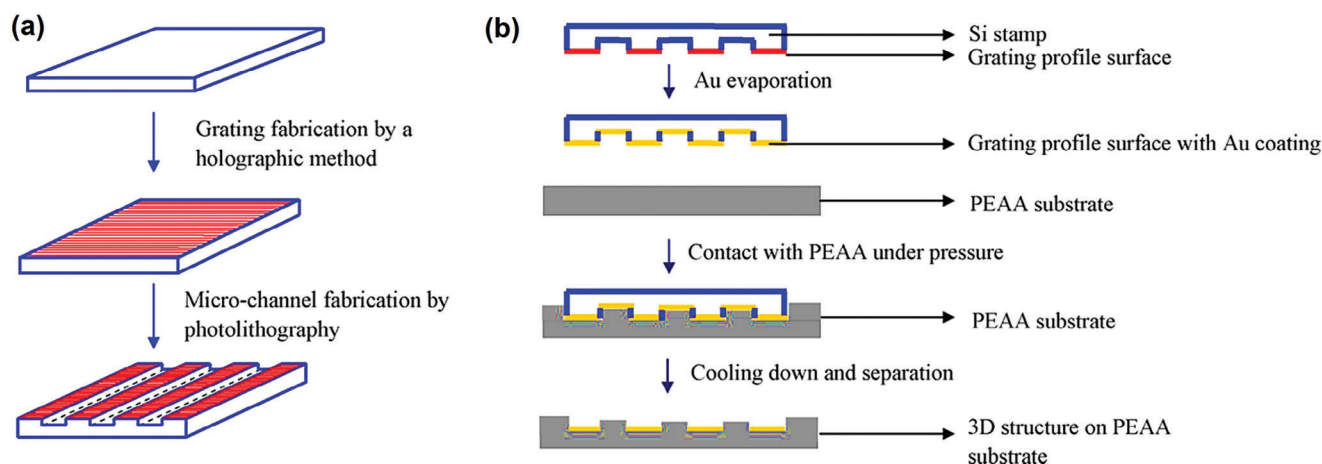


Figure 8. Schematic representation of stamp fabrication and microstamping processes. Reproduced with permission from.^[33] Copyright 2008, Elsevier.

has been used to create the grating structures, due to its excellent metal adhesion property compared to its counterparts like polystyrene, polycarbonate, and poly(methyl) methacrylate.^[33] First, a silicon stamp was fabricated by combining holographic methods and photolithography, and then the micro-channels, grating coupler, and thermally evaporated Au were transferred to the PEAA substrate in a one-step stamping process, as shown in **Figure 8**. The microchannel had been designed considering the spot size of the LASER beam used to illuminate the sample. For instance, the microchannel had been made of 100 μm with 3 mm given between each channel, as the LASER spot was 2 mm. The transferred structural characteristics have been assessed and validated using AFM studies, and the sensor characteristics have been determined by coating a layer of mercapto-PEG onto the sensor surface.

The aforementioned examples showcase the transformative potential of the NIL process in developing GC-SPR platforms. However, NIL confronts certain challenges, including the sub-nanometer resolution demanded for the upcoming advanced plasmonic platforms. Another consideration is the throughput of the fabrication process, where conventional NIL methods encounter impediments in scaling for large-scale production. Ongoing research focusing on high-throughput NIL techniques such as roll-to-roll or step-and-flash lithography is actively addressing this limitation.^[36]

4.3. UV Lithography- Mask-Based Approach

UV lithography, a photolithographic process that harnesses the power of short wavelength UV light to selectively expose and pattern a photo-resist-coated substrate, can be used to create intricate structures. UV lithography is of high interest for the fabrication of GC-SPR due to its ability to achieve high-resolution patterns on a given substrate. Long and co-workers, presented a fabrication method that utilizes standard UV lithography to fabricate GC-SPR sensor chips.^[29] Such a fabrication scheme would offer the possibility of high throughput fabrication using well-established cleanroom processes. For instance, glass substrate had been used as a substrate material for the fabrication follow-

ing processes. In the first step, a positive photoresist has been spin-coated onto the substrate, followed by patterning using standard optical lithography. After a development process, a SiO_2 film was evaporated onto the patterned substrate. A lift-off process has been carried out to create the grating structure. Finally, a 130 nm thick aluminum film was evaporated on the SiO_2 grating.^[29] This process resulted in the formation of Al grating structures with a period of 6733 nm and a depth of ≈ 202 nm in a rectangular profile.

4.4. Electron Beam Lithography-Based Approach

In general, the fabrication of GC-SPR chips is based on the 3D shaping of a surface to create a grating structure.^[59] However, Saito and co-workers presented a fabrication approach to realize a GC-SPR chip with a flat surface. This approach integrates the grating structure into the bulk/interface region of the SPR chip. Here, the grating structure was processed on a silicon-on-insulator (SOI) substrate (top thickness 700 nm, buried oxide (BOX) thickness 1000 nm, and handle wafer thickness 750 nm) and transferred to a polymeric substrate resulting in a flat sensing surface.^[22] In the first step, an electron beam lithography process has been carried out to create the pattern of the grating structure. Then, the resist pattern was transferred into the top silicon layer of the SOI substrate using a deep reactive ion etching. A second dry etching process has been carried out to define the resulting height of the silicon-based gratings. After the thinning process, the wafer has been coated with a 60 μm thick SU-8 layer, and a 500 μm thick glass cover has been stacked onto the SU-8 layer. To finalize the GC-SPR chip, the handle wafer and the BOX layer have been etched away in the grating area. Subsequently, a 30 nm Au layer was deposited on the flat silicon/SU-8 surface.

4.5. Lithography-Free Approach

A simple sinusoidal-shaped GC-SPR chip can be fabricated using a recordable Blu-ray disc (BD-R) without the need for

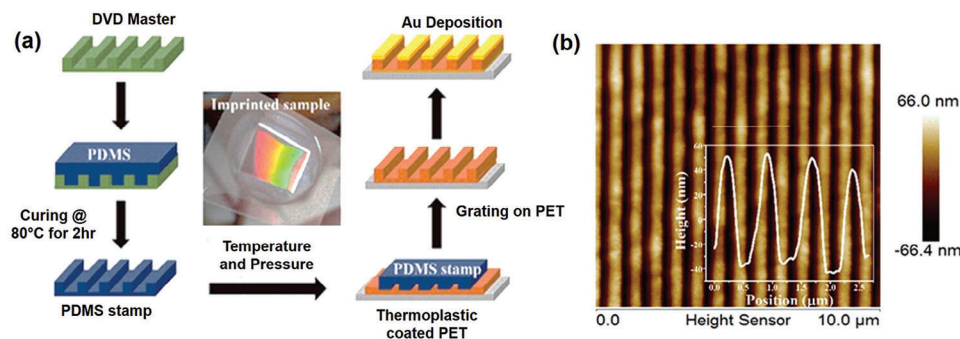


Figure 9. A) Schematic representation of different steps involved in the fabrication of GC-SPR using DVD as a master. B) AFM images of gold coated sample with an inset showing the height profile of the gold gratings. Reproduced with permission from.^[64] Copyright 2019, Elsevier.

expensive nano fabrication tools and clean room facilities.^[60] First, the disc can be cut into small samples using a scissor. The protection layer covering the grating layer can be removed with a tweezer. To finalize the grating coupled SPR chip, a thin metal layer (e.g., 50 nm of Ag) can be deposited on top of the grating. Such fabricated GC-SPR chips have a reported grating period of 314 nm and a depth of 20 nm.^[29] Using a DVD-R disc as a nanoimprint stamp to imprint the structure onto a PDMS substrate with subsequent metal evaporation can yield high-throughput fabrication of low-cost sinusoidal-shaped GC-SPR chips.^[61] Compact disc (CD)-based grating coupled SPR devices have the possibility to produce low-cost grating-coupled SPR sensor chips with well-characterized optoelectronic characteristics.^[62,63]

Another lithography-free fabrication process to realize GC-SPR chips has been reported by Yeh et al.^[35] Here, the authors have used the surface buckling of a PDMS film after an oxygen plasma treatment. PDMS sheets were cut into 25 × 75 mm substrates, bent along their long axis, and clamped in a circular fixture. Then, the elastomeric substrate was exposed to an oxygen plasma for 4 min. Afterward, the circular fixture was removed and the PDMS was allowed to get back to a planar shape. This process results in the buckling of the PDMS surface, producing a sinusoidal surface shape. Here, the amplitude and pitch of the structures vary along the substrate surface. To finalize the GC-SPR chip, a metallization process can be carried out to coat the substrate with a metal layer (e.g., Au). Yeh and co-workers, reported the use of a chirped diffraction grating on poly(dimethoxysilane) with spatial variation in both pitch and amplitude along its surface. Also, a thin silicon oxide layer was coated onto the grating structure for evaluation. The chirped pattern is anticipated to provide varying SP coupling along the surface of the sample, which had been characterized by measuring the ratio of transmitted p and s polarized light (nominal value of 1 without gratings). Similarly, Mohapatra and his co-workers in 2020 utilized the grating structures in the DVDs to develop a GC-SPR for sensing polar solvents, as shown in **Figure 9**.^[64] The grating sinusoidal grating structures were transferred to the PDMS stamp and then to thermoplastic polymer-coated polyethylene terephthalate. The fabricated grating structure has been characterized to have the following surface features, including the line width and periodicity of 542 and 731 nm, respectively. A Au film thickness of 60 nm has been

utilized as a plasmonic layer resulting in a sensitivity of ≈ 535 nm RIU⁻¹.

The list of approaches reported in the literature to fabricate grating structures on different substrate materials is consolidated in **Table 3**, along with the sensitivity values to assess the performance of standards. Subsequently, in **Table 4**, the key features of these approaches are compared to provide valuable insight into selecting the appropriate approach for the specific application.

5. Material Composition

GC-SPR chips can be fabricated using different materials. In the following section, an overview of different substrate and plasmonic materials, which have been used in the fabrication of GC-SPR chips will be presented. This section will also discuss the pros of cons of the materials being utilized for the development of GC-SPR.

5.1. Substrate Material

A common material combination for SPR chips is glass substrates combined with an Au layer (and a thin adhesion layer, e.g., Ti or Cr). Generally, glass substrates can be combined with polymer layers (e.g., fluoropolymer) to obtain grating structures on the surface via nanoimprinting and subsequent metal deposition. Such materials can be combined in a glass/Au/fluoropolymer/Au layer structure.^[57,58] A double metal deposition process with a lift-off process of the second layer can result in a glass/metal (e.g., Au + adhesion layer) material combination. Here, the grating structure is directly integrated into the metal layer without the need for imprinting processes or intermediate polymer layers.

Polymeric materials can also be used as substrates for GC-SPR chips. As discussed above, CDs and DVDs are potential substrates for GC-SPR chips due to their reproducible grating structures. Here, such substrates are typically coated with a thin metal film. Another polymeric substrate that is used for such applications is PDMS. After imprinting and curing, a metal film can be deposited on the PDMS layer. Here, a PDMS/metal interface is created. Despite the substrate material being used, the

Table 3. List of various approaches used to fabricate GC-SPR along with the grating materials and the geometric features.

Approach	Grating material	Grating period	Sensitivity	Refs.
Master mold holographic method, and elastomer stamping-soft lithography	Polymer NOA-72	457 nm	160 deg RIU ⁻¹	[18]
Silicon grating -based GC-SPR chip	SOI-wafer + cover glass	1050, 1150, and 1250 nm	–	[22]
Laser interferometry lithography to from PDMS mold and nanoimprinting	Microscopic glass coated with thiolene resin film (NOA 61)	500 nm	193 deg RIU ⁻¹	[25]
Laser interference lithography	Glass	400 nm	100 cells mm ⁻¹	[26]
Laser interference lithography + metal lift-off	Microscope slide (Glass)	396 +- 4 nm	–	[28]
BD-R/DVD-R -based GC-SPR chip	BD-R/DVD-R	314 nm	319.96 nm RIU ⁻¹	[29]
CD-R -based GC-SPR chip	CD-R	1470 nm	1477.74 nm RIU ⁻¹	[29]
UV nanoimprint	Glass slide with UV curable polymer (NOA 72)	500 nm	–	[32]
Micro-stamping	PEAA	500 nm	–	[33]
Buckling of PDMS following oxidation	PDMS	chirped	–	[35]
Roll-to-roll nanoimprint	PET	200 nm	210 nm RIU ⁻¹	[36]
Nanosecond laser interference lithography	Silicon	1120 nm	961.5 nm RIU ⁻¹	[37]
Molding process	Plastic	508 nm	95 deg RIU ⁻¹	[38]
UV imprint	Glass slide coated with OG	552 ± 5 nm	285 nm RIU ⁻¹	[39]
Laser interferometry lithography from PDMS mold and nanoimprinting	Microscopic glass coated with thiolene resin film (NOA 74)	500 nm	–	[42]
Nanoimprint	Fluoropolymer	510 nm	119 deg RIU ⁻¹	[58]
Silicon grating master mold – deep reactive ion etching	PDMS	833 nm	321.78 nm RIU ⁻¹	[65]
DVD-R -based GC-SPR chip	DVD-R	320 nm	–	[66]

crucial parameter that influences the SPR is the RI of the substrate. For instance, Anju and co-workers., studied the influence of three different substrate materials on rectangular self-referenced GC-SPR using TiO₂ gratings, as shown in **Figure 10**. The substrates studied include CaF₂, SiO₂, and BaF₂ with RIs 1.4263, 1.4447, and 1.4662, respectively.^[52] As discussed in section 3.2, it is known that rectangular gratings give rise to two distinct reflectance minima, the name reference spectrum, and the SPR spectrum. The reference spectrum is due to the generation of SPs at the Au–substrate interface and the SPR spectrum is from Au-medium/analyte interface.

The results showed that an increase in the RI of the substrates shifted the reference spectrum toward longer wavelengths, while the SPR spectrum has been negligibly affected. Furthermore, the sensor performance has been evaluated by comparing the signal-to-width ratio (SWR), which is calculated as the ratio of the difference between the peak reference wavelength and the SPR wavelength to the FWHM of the SPR peak. The SWR results have shown that the CaF₂ has a better SWR, however, it involves a limitation in the experimental design demanding a broadband light source and a compatible spectrometer. In summary, it could be noted that the selection of the substrate

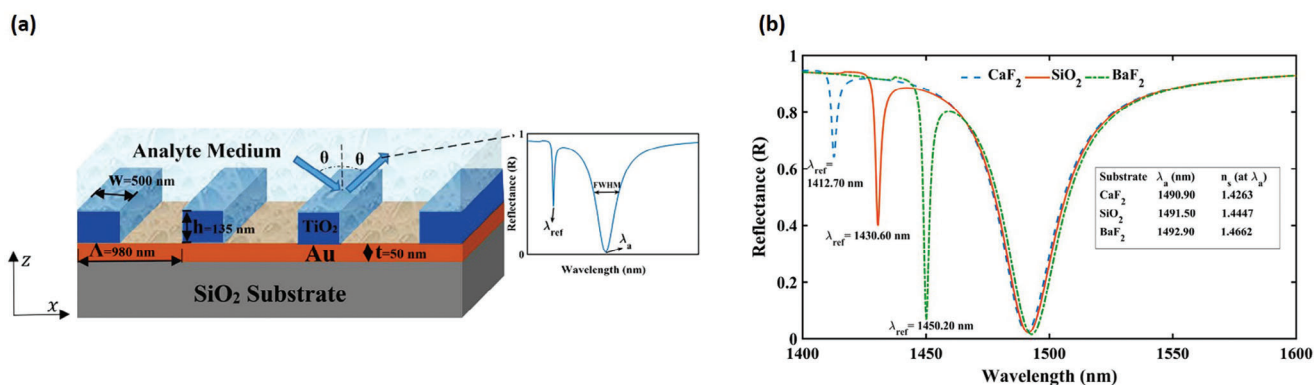


Figure 10. A) Schematic representation of TiO₂-based self-referenced rectangular GC-SPR system. B) Simulated reflectance curves of the TiO₂ gratings on different substrates with varying RIs. Reproduced with permission from.^[52] Copyright 2019, Optical Society of America.

Table 4. Comparison of key features of various approaches used to fabricate GC-SPR.

Fabrication technique	Resolution	Uniformity	Grating quality	Feature shape control	Defect rate	Reproducibility	Material Compatibility	Key advantages	Key disadvantages
Interference lithography	Sub-micron (100–500 nm)	Good over large area	High	Limited to sinusoidal gratings	Low	High	Works well with photoresists	High quality for large area	Requires precise alignment and high-energy lasers
Nano-imprint lithography	Nanoscale (10–100 nm)	Depends on mold quality	High	Limited to the mold structure	Low to moderate	Excellent	Wide range including polymers	Cost-effective and suitable for flexible materials	Limited to mold quality and durability
E-beam lithography	Nanoscale (<10 nm)	Excellent Small area	Excellent	Arbitrary shapes possible	Very low	Moderate (Long write time)	Limited to e-beam resists	High precision and resolution	Complex, time-consuming, and expensive
Mold-casting	Limited to micron scale	Moderate	Moderate	Limited to mold structure	Moderate	High	Wide range of materials/polymers	Simple and low-cost for large areas	Limited resolution and potential for defects in the mold
UV-lithography	Sub-micron (300–500 nm)	Good	High	Limited to simple structures	Low	High	Limited to UV-sensitive materials	Good resolution and a relatively fast	Requires UV-sensitive materials and precise control of exposure
Roll-to-Roll printing	Limited to micron scale	Moderate	Moderate to high	Limited to simple structures	Moderate	Excellent	Excellent for flexible substrates	High throughput and cost-effective for large areas	Limited by resolution of the printing process

materials for GC-SPR plays a pivotal role in influencing the sensor performance. Furthermore, these insights provide a foundational understanding for optimizing and tailoring GC-SPR substrates.

5.2. Plasmon Active Material

GC-SPR chips generally contain a micro or nano grating structure combined with a plasmonic material.^[67] In most cases, plasmonic materials such as thin Ag and Au films are typically used. Even within Ag and Au, the choice of material has been found to influence the sensitivity of the GC-SPR.^[68] For instance, Su and co-workers 2016 reported that the Ag of similar geometric features has a superior performance compared to Au.^[41] Ag films always outperform Au films due to the least amount of Ohmic loss and inter-band transition loss. Despite the superior sensitivity, chemical instability is the major challenge in utilizing Ag as a plasmonic material. In order to overcome the oxidation of Ag film, it has been suggested to use a bimetallic grating structure with 47 nm of Ag and 3 nm thick Au to achieve a sensitivity of 191.8° RIU⁻¹. In contrast, the Ag film exhibited a sensitivity of 193.9° RIU⁻¹. The reported results imply negligible sensitivity drop while the Ag film is still chemically protected. It is also important to note that Su and his co-workers also reported the performance of the GC-SPR through a numerical simulation - based on rigorous coupled-wave analysis (RCWA) for bimetallic structures with aluminum (Al). Briefly, 27 nm of Al with 3 nm of Ag and Au have been reported with a sensitivity of 245.3 and 245° RIU⁻¹, respectively.^[69]

In addition to traditional Ag and Au thin films, some alternative materials have also been presented in the literature.^[70] One such alternative metal-based plasmonic material is aluminum (Al). As shown by Long and co-workers^[29] a 130 nm thick Al film on top of a SiO₂-based grating can be used to realize GC-SPR chips. Al as a plasmonic material is not only attractive due to a cost reduction (compared to noble metals such as Au or Ag) but also due to its high reflectivity, and excellent strength-to-weight ratio. However, similar to Ag, under normal conditions, Al forms a protective aluminum oxide (Al₂O₃) layer affecting the sensitivity of the GCSPR system over time. On the other hand, this layer could be used for the purpose of surface chemistry (e.g., silane chemistry) and subsequent covalent binding of receptor molecules for biosensor applications. In addition, Al does not support SPR as effectively as Au and Ag, and high-precision grating structures in Al can be complex and cost-effective offsetting the material cost.^[71–74] Similarly, Yeh and co-workers have proposed a different plasmonic material configuration. In their work, they have used an Au layer coated with a dielectric layer-based on SiO₂. According to their findings, the SiO₂ layer resulted in a wavelength shift in the transmission peaks. Furthermore, the magnitude of the wavelength shift has been found to be a function of the dielectric layer thickness. Such a surface could serve as an information-rich optical sensor. Furthermore, SiO₂ layers on top of a metal layer could also be used for the well-known silane-based surface chemistry to realize specific biological receptors for biosensing applications. Hence, the choice of the plasmonic material is crucial and determined considering the targeted

Table 5. List of various plasmonic materials and grating structures reported for the development of GC-SPR.

Base material/Substrate	Plasmonic material	Type	Thickness (plasmonic)	Refs.
Glass	Au	sinusoidal	100 nm	[18]
Polycarbonate (DVD)	Al	Sinusoidal	80 nm	[21]
Quartz	Au	Sinusoidal	50 nm	[25]
Glass	Cr/Au	Rectangular	5 and 40 nm	[28]
Glass substrate coated with a UV-curable polymer	Cr/Au	Sinusoidal	2 nm/70 nm	[32]
PEAA	Au	Rectangular	150 nm	[33]
PDMS	Au	Sinusoidal	≈ 40 nm	[35]
PET	Au	Rectangular	30 nm	[36]
Silicon	Ag	Sinusoidal	50 nm	[37]
Plastic	Au	Sinusoidal	100–150 nm	[38]
Glass (ZF2)	AlF ₃ /Au	Sinusoidal	1500 ± 5 nm/45 ± 5 nm	[39]
SiO ₂	Ag (Ag) thin film with Si ₃ N ₄ grating	Rectangular	Ag 40 nm	[51]
SiO ₂	Au (Au) thin film with TiO ₂ grating	Rectangular	Au 50 nm	[52]
Glass	Au	sinusoidal	40 nm	[65]
–	Al/Al–Au/Al–Ag	Rectangular	30 nm/27 nm– 3 nm/27 nm–3 nm (simulations)	[69]

application, chemical stability, surface chemistry, and required sensitivity. **Tables 5** and **6** provide a comprehensive view of various substrates and the plasmonic materials reported in the literature along with their grating topography.

6. Applications of GC-SPR

The primary focus of research in biosensing technologies relies on the detection of an analyte accurately in a given sample through their interaction with an immobilized ligand on a transducer element. Several approaches, including optical, electrical, electrochemical, and piezoelectric techniques, are being explored to realize a sensitive biosensor technology with remarkable de-

tection limits and specificity.^[77] Among these, optical sensing technologies especially SPR and LSPR-based technologies offer prospective advantages, rapid real-time analysis with high capabilities of multiplexing and miniaturization^[78,79] Here, we briefly discuss specifically the applications of GC-SPR reported in the literature. GC-SPR has always been a choice to explore due to its advantages, including sensitivity, reproducibility, quantitative readout, parallel analysis (SPR imaging^[80]), and is a label-free method. From the user's point of view, label-free sensing is highly preferred due to its ease of utilization and fast response. However, the detection limits, sensitivity, and specificity largely depend on the analyte being sensed, the ligand immobilized on the sensor surface, and the detection setup used.

Table 6. Comparison of key features of different materials used to fabricate GC-SPR.

Material	Sensitivity	Stability	Fabrication ease	Scalability	Cost	Key advantages	Key disadvantages	Refs.
Au	Very High	Excellent	Moderate	Good	High	High sensitivity, excellent stability, and Biocompatible	Expensive, soft, prone to mechanical damages	[72]
Ag	Excellent	Poor	Moderate	Good	Moderate	Highest sensitivity with sharp resonance curves	Oxidizes easily and requires a protective coating	[41]
Al	Moderate	Good	Easy	Excellent	Low	Cost-effective, easy to fabricate, and good for large-scale production	Lower sensitivity than Au/Ag. Also forms an oxide layer	[75]
TiO ₂	High	Excellent	Moderate	Good	Moderate	High stability, Biocompatible with high RI	Lower conductivity than metals and involves a complex fabrication process	[52]
Stainless steel	Moderate	Excellent	Easy	Excellent	Low	Cost-effective, durable, and Corrosion-resistant	Lower sensitivity than noble metals and limited resolution	[15]
Graphene	Very High	Good	Challenging	Limited	High	Ultra-thin, high conductance, and tunable properties	Fabrication difficulties and large-scale production with uniformity	[76,50]

The analyte of interest may vary among biomolecules, organic compounds, small molecules, chemicals, and heavy metals, depending on the intended application. The following section focuses on biomolecule sensing, especially for clinical diagnostics. The scientific advancement in the field of computational biology led to pioneering improvements such as next-generation genome sequencing, high-throughput antigen screening, and small-molecule docking. Successively, the improved technologies have led to a better understanding of disease pathogenesis at the molecular level and the identification of potential molecular biomarkers. Traditionally proteins and nucleic acid sequences are widely used as molecular targets in clinical diagnostics owing to their established interaction mechanisms. Recently, other biomolecules such as lipids, peptides, hormones, organic compounds, and small molecules have also gained momentum in clinical applications. This section summarizes a few reported applications of GC-SPR for the detection of biological macromolecules such as proteins, nucleic acids, lipids, and so on. Finally, an insight on multiplexed, high-throughput screening will be discussed.

6.1. Detection of Protein Biomarkers Using GC-SPR

Proteins are structurally and functionally complex macromolecules performing crucial intra- and extracellular functions. Proteins are chains of amino acid sequences linked through peptide linkages.^[81] The amino acid sequences through peptide linkages form a linear peptide sequence, which is later folded to create secondary and tertiary structures. Almost all functions of the living cell are controlled through protein interaction and maintain the homeostasis of a living organism. Hence, proteins are often utilized as biomarkers due to their established role in several physiological and pathological conditions. In general, these proteins are detected using immunological methods. The basic principle of the assay depends on the formation of the antigen-antibody (protein-protein) complex. Early methods of immunological diagnosis involved precipitation reaction, where either antigen or antibody is allowed to diffuse to the other on an agar matrix and investigated for the formation of a visible precipitate. Later it was improved by applying an electrophoretic field, termed counter immunoelectrophoresis (CIE). However, these methods require a high concentration of antigen-antibody to form a visible precipitation line. To overcome such limitations, labeled assays were developed, where the antibodies (mostly) were attached with labels to improve the quality of the testing. The label can be a fluorescent dye (fluorescein isothiocyanate (FITC), immunofluorescence assay), radioisotope (radioimmunoassay, RIA), or an enzyme (enzyme-linked immunosorbent assay, ELISA).^[82–84] The labeled assay can be in a direct or indirect format. In the case of a direct format, the specific antibody is coupled to a label, whereas in the indirect format, the antigen and the specific antibody interaction are detected in an additional step using a labeled antibody that binds to the specific antibody. In addition, there are other ingenious variations of such “sandwich” assay formats, where the antigen is trapped between two antibodies, namely capture and detection antibodies (labeled), and competitive immunoassay, where two antigens compete for a single antibody. These molec-

ular techniques are found to be more sensitive than conventional culture-based methods and microscopic methods. However, despite the inherent limitations of handling labeled reagents, label-free formats are highly preferred for end-user applications. In this review, we will discuss a few GC-SPR systems reported for protein biomarker detection using labeled and label-free formats.

Tawa and his co-workers in 2015, utilized Ag and Au-based GC-SPR for the detection of alpha-fetoprotein (AFP) in a labeled sandwich immunoassay format using surface-plasmon field-enhanced fluorescence.^[31] It is important to note that the Au and Ag-based grating structures were overlaid with a silica layer of ≈ 20 nm to sufficiently suppress fluorescence quenching of the fluorescent labels. In brief, the grating structure used was as follows, the pitch, groove depth, and duty ratio were 430, 30, and 0.5, respectively. The experimental setup consisted of a laser beam of 637 nm from a laser diode attached to a rotational arm that passed through the band-pass filter and polarizer. The polarized light source illuminated the grating structures, which were horizontally placed on the sample stage at the rotational center. The reflected light had been monitored using a CCD detector. The fluorescence has been measured using a photomultiplier tube with an emission filter mounted on the same arm as that of the CCD detector. A cylindrical aperture placed in front of the CCD detector played a vital role in preventing stray reflected or scattered light from falling on the CCD. For Au chips, the surface plasmon coupled emission (SPCE) has been detected for AFP between 200 and 10 pg mL⁻¹, while for Ag, it has been shown to detect as low as 2 pg mL⁻¹. It has also been shown that the Ag plasmonic chip showed five times higher fluorescence intensity than the Au plasmonic chip. The LoDs had been shown to be 8 and 20 pg mL⁻¹ for Au and Ag plasmonic peaks, respectively. Despite high fluorescence intensity, Ag chips showed inferior detection limits than Au chips due to the limitations of the experimental setup, as the incident and the detection wavelength bands were close, leading to a large background. Further, the setup had been modified to improve the detection limit to 4 pg mL⁻¹ for Ag chip.

Similarly, in 2019, Kotlarek and his co-workers reported the use of GC-SPR for the label-free detection of thrombin in human blood plasma down to nanomolar concentrations.^[85] The diffraction chip consisted of a periodically corrugated Au film where antifouling poly[(N-(2-hydroxypropyl)-methacrylamide)-co-(carboxybetaine methacrylamide)] (poly(HPMA-co-CBMAA)) brushes were grafted and functionalized with capture aptamers (Figure 11). The polymeric brushes have been found to be effective in inhibiting the non-specific adsorption of protein from forming biological matrices like blood, plasma, and saliva. The reported work utilized a single-stranded DNA aptamer as a capture probe that specifically binds to the exosite 1 of thrombin through the formation of a G-quadruplex. The optical setup developed in-house included, a polychromatic light source coupled to a Y-optical splitter, the light from the Y-out arm was collimated using a lens and normally illuminated on a corrugated sensor surface with an asinusoidal grating period of 434 ± 16 nm and corrugation depth of $h \approx 29.5 \pm 3.5$ nm. The grating structure had been coated with polymer brushes and the corrugation depth had been reduced to 13.2 ± 1.6 nm with reduced roughness topography. The sensitivity with and without polymer brushes had been

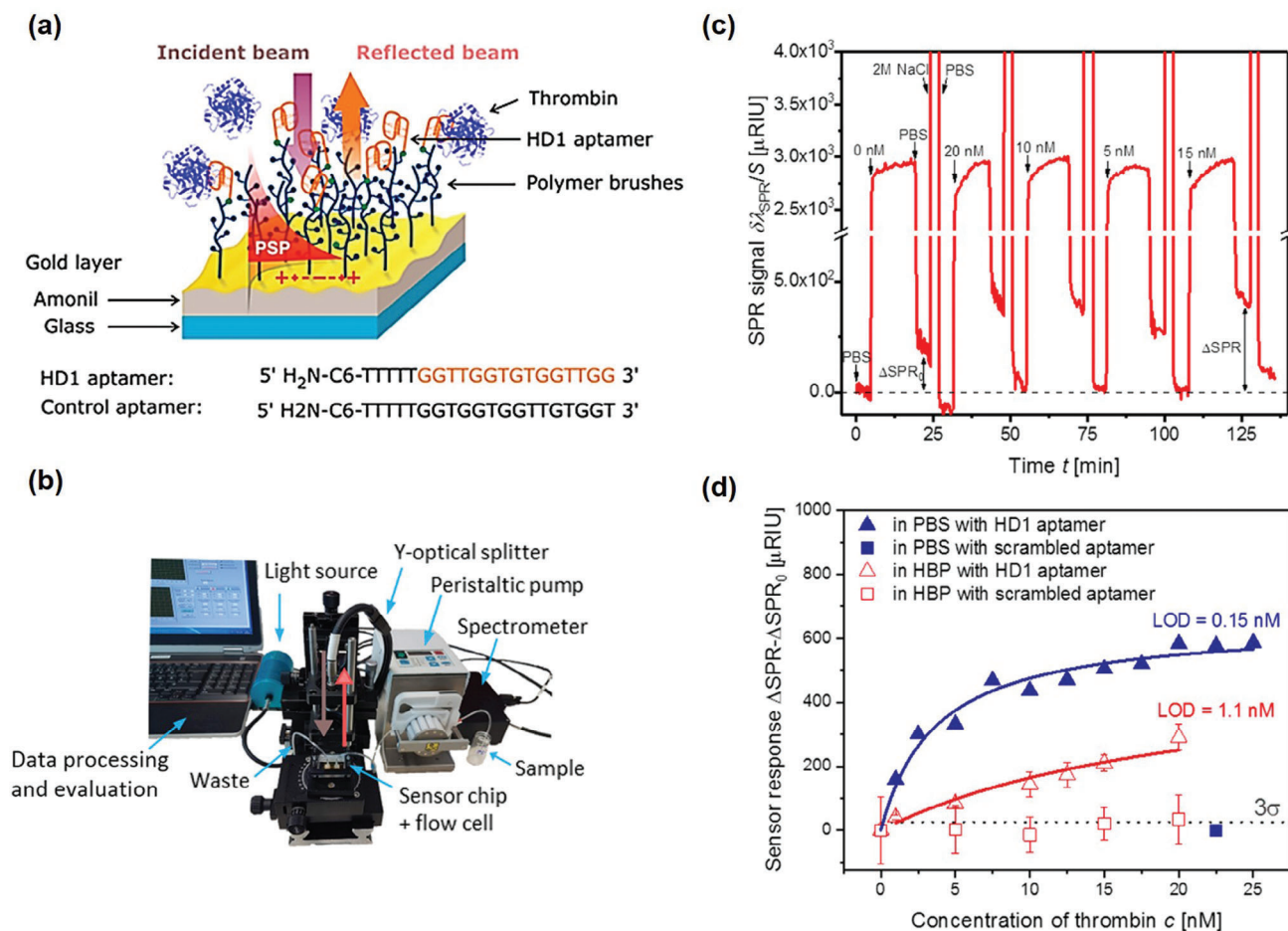


Figure 11. Detection of thrombin: a) Schematic representation of the GC-SPR sensor chip modified with polymeric brushes and aptamers. b) Experimental setup utilized for the measurement. c) Real-time monitoring and d) the corresponding dose-response curve of varying concentrations of thrombin in a given sample matrix (PBS and plasma). Reproduced with permission from.^[85] Copyright 2019, American Chemical Society.

evaluated and found to be 459 ± 20 and 238.3 ± 5.4 nm RIU⁻¹, respectively. The reduced RI sensitivity had been attributed to the polymer brushes occupying part of the evanescent field. The LoD obtained using this developed GC-SPR sensor chip had been found to be 0.15 and 1.1 nM of thrombin in the PBS buffer and human blood plasma (HBP), respectively. The detected levels had been found to be in accordance with the clinically relevant values.

The two proteins discussed here largely vary in their molecular weight, which is a crucial parameter determining the sensitivity of a GC-SPR platform. For instance, alpha-fetoprotein is at a larger molecular weight scale, approximately double that of the thrombin. The effect of the molecular weight reflected in the sensitivity reported that thrombin showed a detection limit of 5 ng mL⁻¹, while the alpha-fetoprotein showed 4 pg mL⁻¹ owing to their higher molecular weight. Nevertheless, it is interesting to note that the systems vary in their optical setup; hence, a direct comparison may not necessarily be possible. However, we wish to highlight the importance of molecular protein weight in determining the sensitivity of the GC-SPR-based sensing for efficient sensor design.

6.2. Detection of Oligonucleotides Using GC-SPR

Nucleic acids (DNA and RNA) are the information-carrying molecules of the cells that govern their overall function. Sequencing, detecting, and amplifying nucleic acids have always been of research interest to understand life forms. In this section, we will discuss the significance of detecting nucleic acid sequences in healthcare applications. Nucleic acid detection methods have revolutionized clinical diagnostics due to their high sensitivity and specificity.^[86] In general, specific nucleic acid sequences or genes are targeted to identify or detect pathogens in a given sample, or the expression of a given gene is profiled to mark the onset of a disease. The extensive research in genome sequencing of humans and major pathogens and its widespread availability in computer databases are being used in various applications, including the identification of conserved gene sequences and antimicrobial resistance gene sequences, respectively. The standard method of nucleic acid-based test for the diagnosis involves isolation of nucleic acid material from organisms present in the sample, followed by digestion using restriction endonucleases, gel electrophoresis, and nucleic acid hybridization.

DNA-hybridization is a phenomenon where a single DNA strand interacts with the complementary DNA strand forming a double helix structure. Hence, a probe DNA fragment empirically designed for diagnostic purposes can be labeled and used to detect the presence of a complementary DNA sequence in a given sample. However, often the detection of targeted nucleic acid sequences from body fluids such as blood, sputum, or urine could be challenging due to their lower availability. Here we describe an example of exploring GC-SPR to detect the lower concentration of short oligonucleotide sequences, which is highly essential for clinical diagnostics and genome sequencing. Vala and co-workers in 2010, developed a multiplexed portable GC-SPR capable of detecting ten samples at a time.^[38] Several optimizations, including operating wavelength, angle of incidence, and grating features, have been optimized to achieve high sensitivity. The resolution of the optimized GC-SPR system has been found to be 6×10^{-7} RIU with a LoD of 1 nm for the detection of short oligonucleotides. It is interesting to note that previously, the same group worked on developing a 4-channel system. The primary optimizations were carried out using the commercial grating solver PC-Grate, International Intellectual Group, Inc. Different angles of incidences such as 5, 25, 45, and 65 had been tested with grating periods of 508, 414.2, 358, and 327 nm with modulation depths of 27.8, 22.7, 19.6, and 17.9 nm, respectively. The wavelength of choice had been 760 nm due to the availability of a wide range of narrow-band light sources in the region. The chip-to-chip reproducibility had been found to be 92%. The optimized sensor system had been reported to achieve a resolution of 3×10^{-7} RIU and a LoD of 200 pM for short oligonucleotides. These examples show the potential of GC-SPR systems in detecting short oligonucleotides down to pM concentrations without any nucleic acid amplification steps. More often, the major limitation of nucleic acid detection is the need for an amplification procedure in order to detect short nucleotide sequences. The results show promising evidence that the multiple amplification procedure could be surpassed due to the exceptional sensitivity of the GC-SPR platforms.

6.3. Monitoring of Cell Dynamics

The life cycle of a cell includes dynamic metabolic interactions and complex signaling pathways for proper proliferation. Cellular behavior is highly complex and influenced by external stimuli both in vitro and in vivo. Hence, there is a strong interest in understanding the behavior of living cells to external stimuli for exploring potential drugs, in vitro cell culturing, and regenerative medicine. More often the cellular dynamics are studied using conventional fluorescence microscopy, which is limited by the requirement of labeling and extensive post-processing. Recently, the SPR technologies have been explored to study cell dynamics by exploiting their label-free real-time analysis capabilities. Most often SPR-imaging has been explored for cell biology applications and only a few researchers have tried GC-SPR for live cell dynamics. For instance, Borile and co-workers in 2019 used a GC-SPR sensor platform with a period of 400 nm, a line width of 200 nm, and a corresponding duty cycle of 50%, which was integrated with a PDMS microfluidic channel for cell dynamic study (Figure 12). Particularly, the reported sensor system has been

used for the label-free real-time monitoring of cell adhesion capability and cell-surface interaction, while reducing the medium volume.^[26] The authors have used an experimental setup where the incident laser beam was 633 nm, and the reflected light was collected by a CMOS camera. As discussed in the previous section on experimental configuration, the GC-SPR allowed measurements through phase-interrogation in addition to angle and wavelength-based interrogation, where the SPR resonance is sensitive to the incident polarization of the light. This configuration significantly reduces the requirement of moving parts enabling ease in fabricating point-of-care devices.

Briefly, SHI-1, a human acute myeloid leukemia cell line, had been used to demonstrate the live cell dynamics. The basic principle relies on the phase shift with respect to the cell surface coverage over the gratings facilitating calibration for the quantification of the cell number. SHI-1 cells are a bone marrow-derived myeloid leukemia cell line that usually grows in suspension, but also exhibits adhesion behavior to substrates coated with extracellular matrix proteins. In this particular study, fibronectin has been used as a coating layer for cell adhesion. Apart from establishing a proof-of-concept for real-time monitoring of cell dynamics, this study included several interesting results, first the fibronectin coating provided a passivating characteristic to the surface and significantly inhibited the binding of interfering agents. Second, the Au surface had no influence on the adhesion and viability of the SHI-1 cells, and the detachment of cells subsequent to adhesion using trypsin showed a 79% recovery of phase signal. Third, the optimized sensor platform was found to have a detection limit down to 100 cells mm^{-2} . In addition, the response obtained has also been validated and compared with standard prism-coupled SPR showing a comparable response. Despite the potency of GC-SPR for cell dynamics studies, a few challenges need to be addressed, including the lack of detection of intracellular changes due to limited sensitivity volume, maintaining cell integrity during the experimental procedure, and clogging of microfluidic channels.

6.4. Small Molecules

Similar to nucleic acid and protein molecules for clinical diagnostics, small molecules have gained a remarkable interest in the field of food and environmental monitoring. Bianco and co-workers in 2016, utilized sinusoidal gratings and ssDNA aptamers as capture to detect OTA.^[42] Ochratoxin A (OTA)-L-phenylalanine-N-[(5-chloro-3,4-dihydro-8-hydroxy-3-methyl-1-oxo-1H-2-benzopyrane-7-yl)carbonyl]-(R)isocoumarin (OTA) is a mycotoxin, which often contaminates food and feeds. OTA is also considered to be a potential nephrotoxin with teratogenic, hepatotoxic, immunosuppressive, and carcinogenic effects. This systematic study involved the selection of an efficient capture ssDNA aptamer by comparing four different ssDNA aptamers through QCM. Single-stranded DNA (ssDNA) aptamers had been utilized instead of antibodies due to their stability, ease of production, the feasibility of tagging them with fluorescent molecules, and their cost-efficiency. The biorecognition layer consists of a self-assembled monolayer of mercaptoundecanoic acid (MUA) to which aptamers were immobilized by EDC/NHS treatment, followed by derivatization

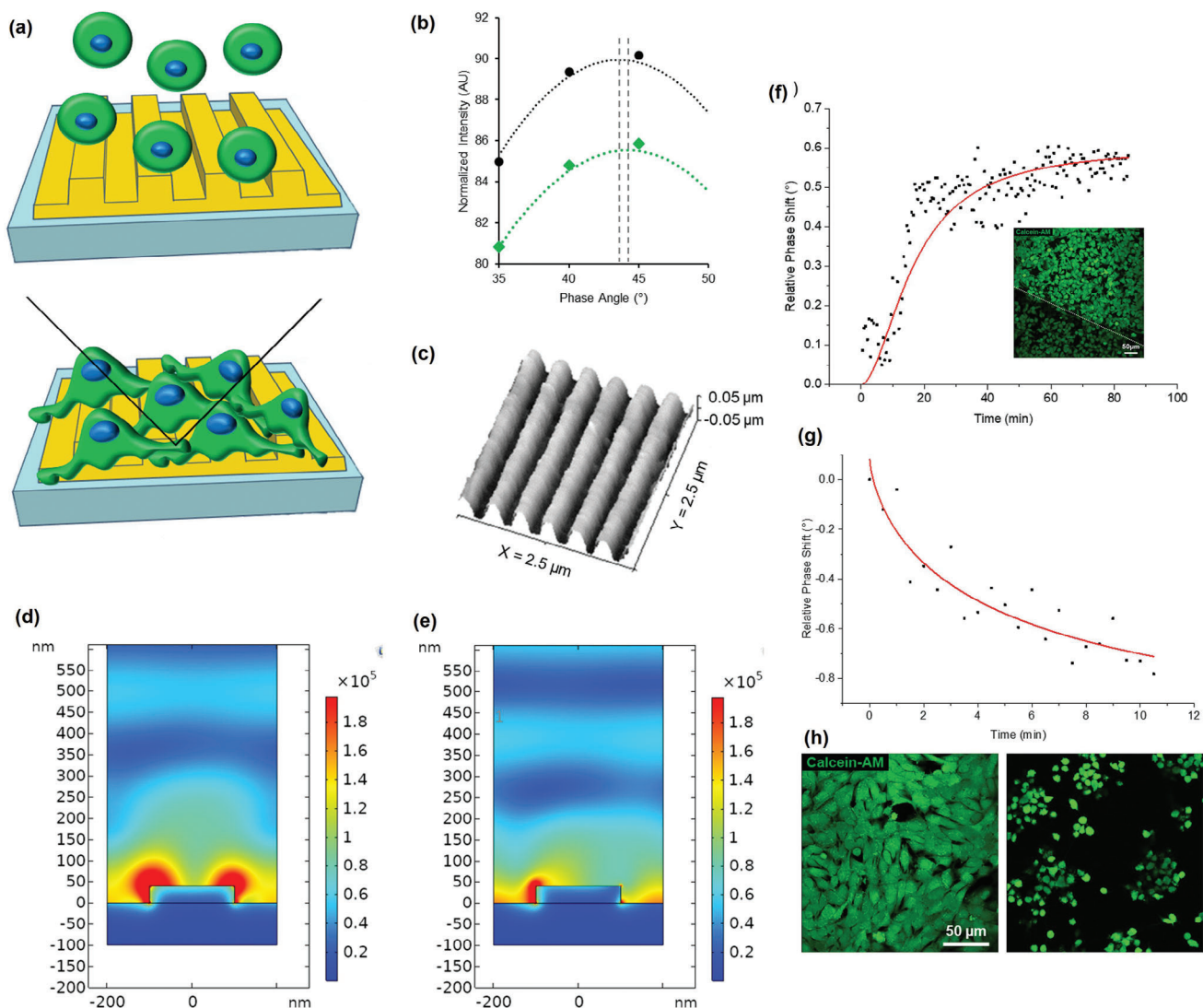


Figure 12. a) Schematic representation of the experimental approach employed to investigate cell adhesion using GC-SPR. Cells in suspension (top) adhere to the gold grating (bottom). The black line illustrates the incident light path, and the reflected light path is utilized for signal detection. b) Polarization spectra details obtained in a no-cell condition (black) and with cells adherent to the surface (green). Gray lines indicate the spectra maximum, calculated by interpolating experimental data (points) to a sinusoidal curve (dotted line). c) Atomic Force Microscopy reconstruction of the grating morphology. d) COMSOL simulations illustrate the field over the grating in water and e) in a medium with the cell refractive index (1.38). f) Monitoring of fibronectin coating on the gold grating through SPR phase angle variation in the microfluidic chamber. Representative data from one of three experimental replicates, with a red Hill fit ($R^2 = 0.98$). Inset: SHI-1 cancer cells after seeding on fibronectin coating, imaged at the interface between the glass (below the dotted line) and the gold grating (above the dotted line). Calcein-AM staining did not reveal differences in cell morphology or shape. g) SPR signal reduction as SHI-1 cancer cells are treated with trypsin for detachment from the grating. The red curve represents an exponential fit of the data, representative of three experimental replicates. h) Representative images of cells loaded with Calcein-AM before (left) and after (right) trypsin administration. Reproduced with permission from.^[26] Copyright 2019, Elsevier.

using 2-(2-pyridinyldithio)ethaneamine (PDEA). Later, the pre-treated substrates were utilized to immobilize the aptamers. Then, the optimized system was explored for the detection of OTA, by subjecting the sensor system to varying concentrations of OTA in a buffer solution. It had been found that the optimized GC-SPR system could detect OTA down to 0.2 ng mL^{-1} with a LoD of 0.005 ng mL^{-1} . These results are outstanding as such due to the establishment of small molecule sensing using

SPR phenomena, which has previously been considered to be a limitation of SPR Systems. The remarkable LoD for small molecule sensing could be attributed to the ligand used in the study. The use of ssDNA aptamers significantly confined the biomolecular interaction within the evanescent field leading to remarkable results. Similarly other biomolecules such as cortisol and creatinine have been detected using the GC-SPR platforms.^[87]

7. Conclusion and Perspective

7.1. Point-of-Care diagnosis

The healthcare sector is changing due to the economic pressures demanding the development of patient-centric, low-cost technologies that eventually reduce costs in the healthcare systems. The advent of point-of-care (PoC) devices aims to screen and treat patients at primary healthcare centers, changing the necessity of expensive technologies. In this regard, GC-SPR-based PoC systems have a promising translational potential.

In addition to traditional nucleic acids and protein-based biomarkers, lipids, and small molecules have also gained significant interest due to their association with several pathological conditions. Commonly, lipids are poorly water-soluble organic biomolecules involved in specific and complex physiological functions within the living system. The lipid molecules are classified as sterols, glycerophospholipids, sphingolipids, and fatty acids. Each of the classified lipids has specific functions, including cell signaling, cellular transportation, and cell membrane formation. Especially, the specific lipid molecules found on cell membranes of microorganisms have gained considerable importance for infectious disease diagnosis due to their abundance in the given sample. For instance, lipopolysaccharides (LPS), which are widely distributed in the cell walls of gram-negative bacteria, are of high clinical interest due to their severe pathophysiological effects in humans like septic shock and organ failure. Zhang and co-workers reported a smartphone-integrated GC-SPR for the detection of LPS down to 32.5 ng mL⁻¹ using synthetic peptides as capturing ligands.^[32]

In the particular report, the authors have utilized the NOA 72 resin to incorporate the grating structure using a PDMS stamp. The PDMS stamp contained the replica of the grating structures, which was transferred from the silicon master. The NOA resin with a grating structure has been coated with a 2 nm Cr and 70 nm Au film. The smartphone spectrometer was calibrated using six different filters, namely 470 ± 20, 482 ± 17.5, 525 ± 20, 536 ± 20, and 670 ± 20 nm bandpass filters and a 550 nm long pass filter. The optical setup utilizing the LED light and the camera (CMOS detector 900 × 50 pixels) of the mobile phone has been reported as follows, the light from the white LED initially passes through an aperture of 0.5 mm followed by a polarizer and a filter holder containing a set of six filters (Figure 13). Then the filter light impinged at the Au-grating at an angle of ≈5°. The reflected light from the Au chip passed through a compact disc with gratings of ≈600 lines mm⁻¹ to spatially disperse the wavelength spectrum through -1 diffraction order, which has been later imaged using the camera. The reflectivity has been calculated by normalizing the raw spectrum obtained with the sensor chip with that obtained using reference mirrors.

Initially, the sensitivity was investigated by the physisorption of a BSA layer onto the Au chip, showing a red shift in the resonant wavelength of ≈8 nm. Then the sensor chips were immobilized with synthetic peptides (KC-13 peptide (KKNYSSSIS-SIHC) as bioreceptors for the specific detection of LPS from *Klebsiella pneumoniae*. The peptide immobilized sensor chips have been challenged with LPS of two different concentrations, 10 and 1000 ng mL⁻¹ for 20 min and subsequently measured with

the smartphone setup showing a shift in the resonant peak of ≈1.46 and 5.66 nm, respectively. Later, by subjecting the sensor probes to varying concentrations of LPS, a detection limit of ≈32.5 ng mL⁻¹ was obtained. However, the signal-to-noise ratio was 3.6-fold lower than the conventional prism-based measurement. Moreover, it is important to note that this GC-SPR system holds high translational potential and could be miniaturized for real-time applications with smartphone integration.

7.2. High Throughput Sensing

Multiplexed analysis has always gained considerable interest in the field of medical diagnostics, especially for fatal human diseases like cancer, which are complex and often include a multitude of intrinsic biomarkers. The most popular and extensively used multiplexed analysis methods in clinical diagnostics are enzyme-linked immunosorbent assay (ELISA) and polymerized chain reaction (PCR). However, due to practical limitations, these methods are presently not employed for analyzing multiple biomarkers; instead, they are used for analyzing multiple samples. Hence, the demand for a rapid, sensitive, specific analytical method capable of detecting multiple biomarkers in a given sample still exists. Dostalek and co-workers reported 216 channels on a single chip and demonstrated the label-free detection of biomolecular interactions.^[18] It had been shown that the angular reflectivity spectra calculated for different modulation amplitudes of a sinusoidal grating showed coupling efficiency increased with the increased grating modulation amplitude. The RI sensitivity has been demonstrated to be 160 deg RIU⁻¹ (1.333–1.364). Biosensing efficiency has been evaluated using BSA monolayers formed on the grating surface using dextran sulfate. The average sensor response with a monolayer of BSA has been found to be 0.94 deg, assuming the BSA monolayer thickness of 4–7 nm corresponds to 1.45–1.5 RI, which corresponds to 0.8–1.9 deg nm⁻¹ RIU. The reader consists of a light source module, scanning optics, and a CCD detector with imaging optics. GC-SPR had been realized with a row of diffraction gratings onto a 2D CCD detector. SPR spectra from rows of diffraction gratings array were sequentially captured. Light from edge-emitting laser diode 635 nm passed through the polarizer and collimating lens and fell on the scanning optics, which formed a convergent beam of light by means of a cylindrical lens which was then focused on a row of diffraction gratings on the sensor chip. As a result, a series of reflected diverging beams propagated back to the scanning optics module, which was collimated by a cylindrical lens and separated from the incident light source by a cube beam splitter. The scanning optics module has been motorized to facilitate sequential scanning of rows of gratings. Despite the lab-based demonstration of a high throughput system, the practical application of such technologies is generally limited due to the lack of complex instrumentation.

7.3. Assistance of Machine Learning

The integration of machine learning (ML) techniques with SPR sensors has emerged as a transformative paradigm, enhancing

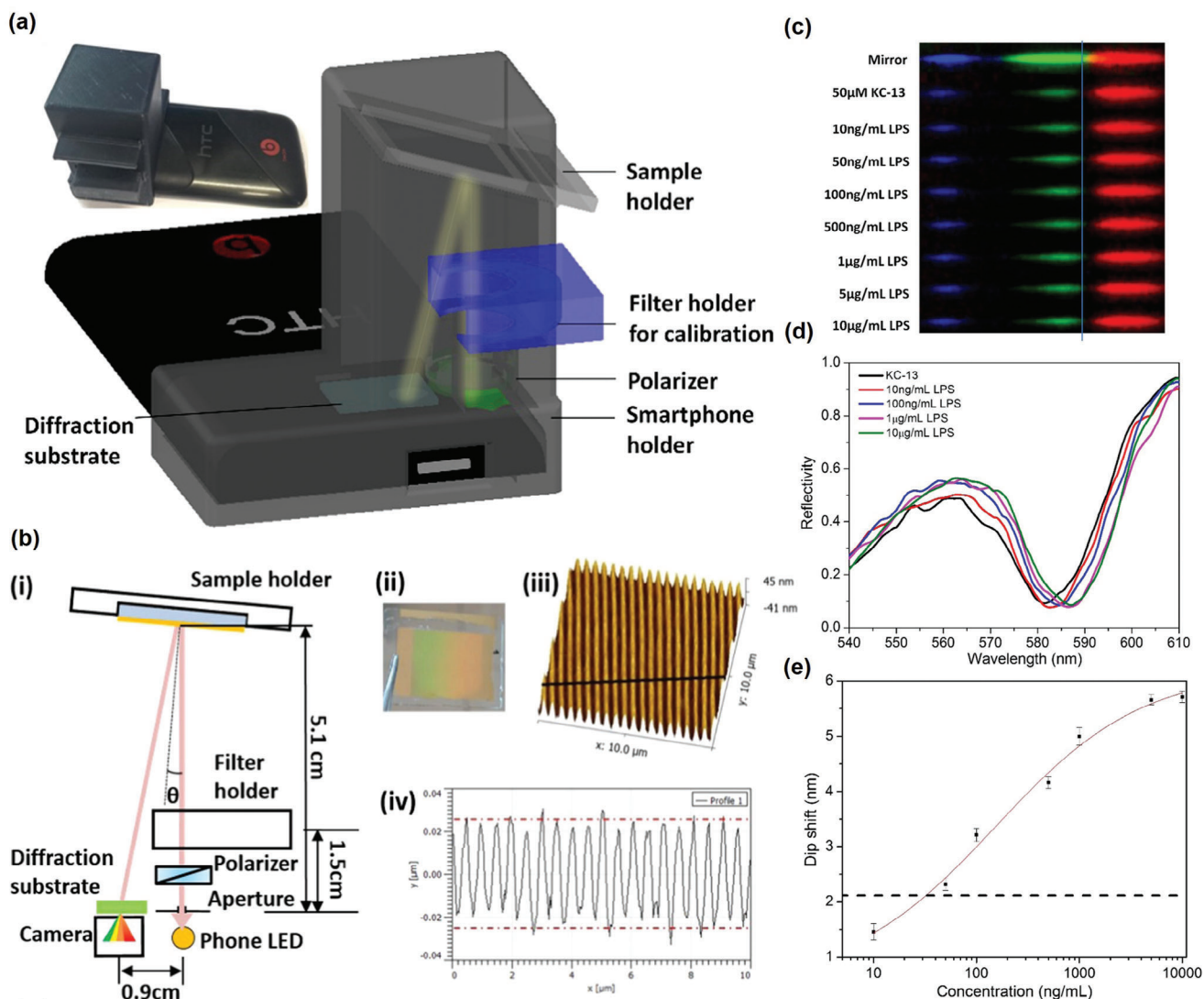
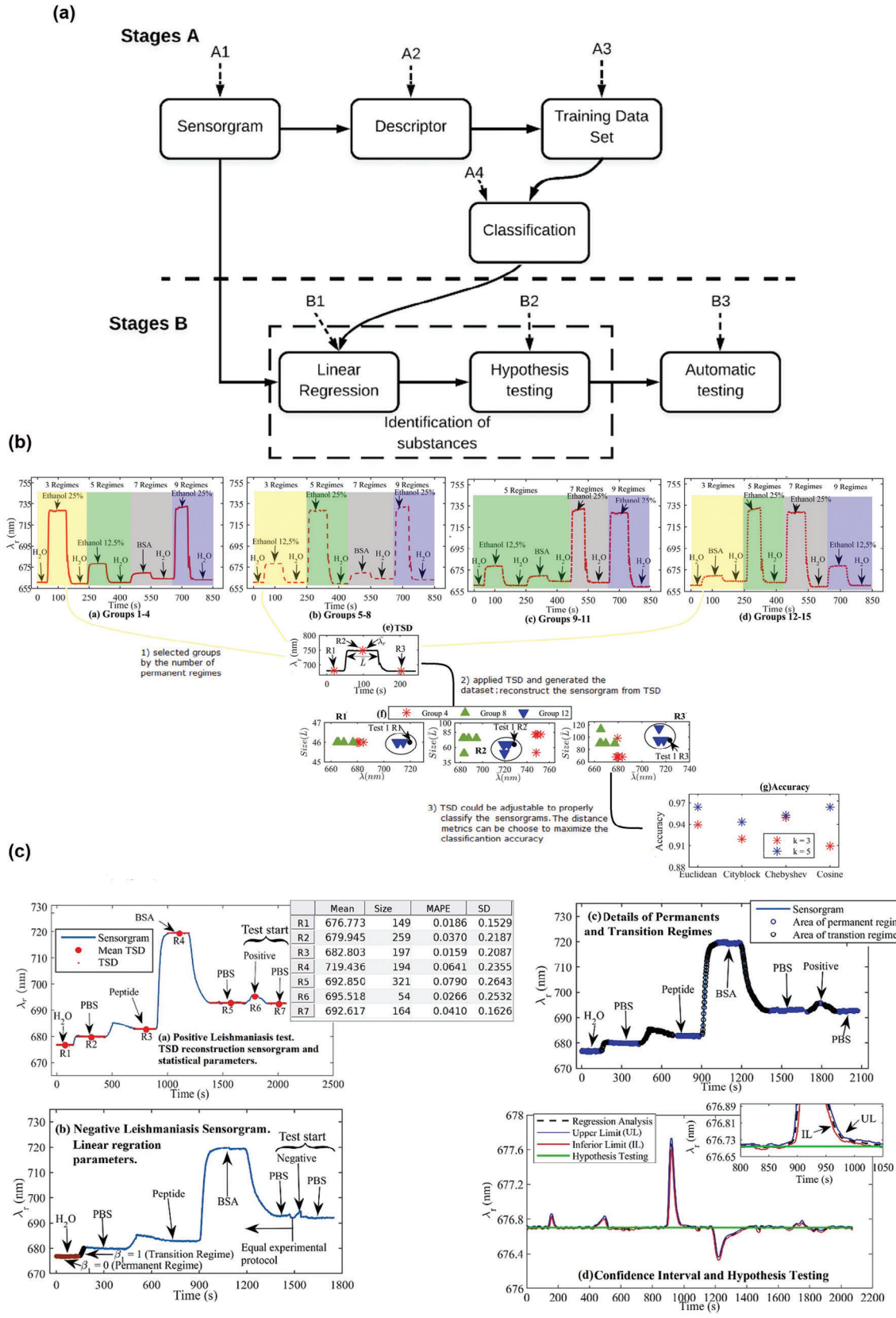


Figure 13. a) Schematic structure of the smartphone spectrometer relying on the in-built LED light, a CD diffraction substrate, and a smartphone camera. Inset is a photo of the 3D-printed plastic sample chamber kit attached to a HTC sensation XE smartphone. b) The optical arrangement of the smartphone spectrometer (i), a photo of an Au sensor chip with diffraction grating (ii), a corresponding AFM image (iii), and surface profile (iv) of the sensor chip. c) Color bands measured on a mirror as a reference and peptide-modified grating Au substrate after incubation with various concentrations of LPS from 0 to 10 $\mu\text{g mL}^{-1}$. The line indicates the SPR resonant band changes. d) The corresponding spectra of grating Au substrate after incubation with different concentrations of LPS. e) The sigmoidal fitted calibration curve (red) with the noise level (dashed black curve) is estimated as three times of the standard deviation of the SPR dip wavelength on 5 different chips. Reproduced with permission from [32] Copyright 2017, Elsevier.

the reliability and efficiency of real-time molecular interaction measurements.^[88] For instance, Julio and co-workers presented an exploration of ML techniques to create intelligent SPR biosensors (Figure 14).^[89] The study introduced a novel ML strategy utilizing the temporal sensorgram descriptor (TSD) and the k-NN algorithm to comprehensively address challenges such as poorly handled samples, instrumentation noise, and molecular tampering. The strength of this approach lies in its holistic methodology, not only classifying sensorgrams but also introducing an Intelligence Module capable of substance identification and automated testing. Particularly the successful application of the ML model in Leishmaniasis diagnosis showcased the practical utility of such ML-enabled SPR biosensors.

Recently, Kushagra and co-workers focused on optimizing the SPR sensor design through a synergistic combination of ML and the particle swarm optimization (PSO) algorithm.^[90] The study highlights the central idea of leveraging ML to forecast sensor performance, leading to an impressive four-order-of-magnitude improvement in optimization speed. The presented results demonstrated the efficiency gains achieved by this ML-PSO conjunction, yielding a tunable SPR sensor with a sensitivity of $68.754^\circ \text{RIU}^{-1}$ and a remarkable FOM of 100. This study underscores the broad potential of ML-enhanced SPR sensors. The intelligent biosensor approach not only addresses practical challenges but also introduces a framework applicable to automated testing and diagnosis. Simultaneously, the ML-PSO



optimization strategy showcases a rapid and precise means of designing tunable SPR sensors, with implications for a range of optoelectronic devices. Importantly, the synergies demonstrated in these studies suggest a promising avenue for the adoption of similar ML methodologies in the analysis of grating-coupled surface plasmon resonance, offering potential breakthroughs in the optimization of diverse plasmonic sensing devices.

In summary, this review article should serve as a reference guide for the understanding and development of future GC-SPR systems. Hence, various aspects of GC-SPR systems, such as theory, fabrication, material composition, design configuration, and potential applications, were discussed in detail. Considering the fabrication process, the essential demand for practical application includes cost, reproducibility, and scalability. In this review, three basic methods of GC-SPR fabrication have been discussed, and here we summarize the merits and demerits of the methodologies.

The use of CDs/DVDs as a substrate for GC-SPR chip fabrication is highly interesting since such substrates provide well-controlled optical grating structures due to their commercial usage in the last decades. Furthermore, such substrates are highly promising because they overcome the dependence on expensive and/or time-consuming lithography processes or microtechnology processes. Despite the ease in fabrication, the crucial bottleneck of using commercially available CD/DVD as substrates for high-throughput fabrication is the need to peel off the metal film. To overcome this limitation a low-cost hot embossing process could be used to structure a flat polycarbonate substrate to obtain grating structures for a GC-SPR sensor chip. Such a fabrication scheme allows a high-throughput and low-cost fabrication of GC-SPR chips. Then, again a silicone mold has to be fabricated using lithographic techniques such as interference lithography or EBL and structured using an RIE process. Hence, an optimal compromise has to be made in determining a fabrication process for using DVD/CD-based substrates. Furthermore, sub-wavelength grating templates and flexible substrates are being explored to enhance the performance of the plasmonic structures.^[68,91,92]

On the other hand, complex lithography techniques are generally used to realize grating structures on a mold or on a substrate owing to their precise structuring. Electron beam lithography (EBL), for instance, is highly interesting due to its maskless patterning nature. However, the long writing time of an EBL process is a major drawback and is, therefore, not compatible with high-throughput fabrication. Alternatively, standard UV lithography allows rapid exposure of photoresists, but the relatively large feature size (down to $\approx 1 \mu\text{m}$) limits its use in the fabrication of GC-SPR chips. Distinctly, nanoimprint lithography (NIL) offers a faster and repeatable process, which is crucial for large-scale

production and particle applications. In addition, NIL could be used for polymeric as well as glass substrates, enabling flexibility in the choice of the material.

In addition to standard lithographic techniques, unconventional techniques such as interference lithography have also been explored for the development of GC-SPR sensor platform. Though the unique technique offers precise formation of periodic lines and space patterns, a wafer scale exposure process is quite challenging due to the need for a precise optical setup. Here, Moa and co-workers and Rodrigues and co-workers presented laser interference lithography setups to enable a wafer-scale process.^[93,94] However, given the promising evidence, the combination of interference lithography with well-established cleanroom processes could provide a low-cost fabrication scheme for GC-SPR chips.^[95] Besides, the choice of fabrication also depends on the structural features of the GC-SPR platforms. It has been shown that the grating period is directly proportional to the sensitivity of the GC-SPR, however, the increase or decrease in the grating structures influences the choice of optical components (light source and detector) and the configuration for the precise measurement of the reflected light. Furthermore, the incorporation of 2D materials and nanostructures has also been found to enhance the performance of the GC-SPR characteristics.^[96–99]

Hence, apart from the fabrication process, the advancement in GC-SPR is facilitated through advancement in the fields of optical instrumentation, microfluidics, nanostructuring, light source, and detector technologies. The light source utilized for establishing the sensor plays a crucial role in determining the sensitivity, configuration, and data acquisition methodology. The light source technology is advancing starting with the invention of incandescent light to the recent organic light-emitting diodes (OLEDs). Unlike lasers, which are widely used for SPR technologies, the later OLEDs/LEDs offer room-temperature processing, large-scale production on flexible substrates, and miniaturization to develop portable devices. The choice of the light source also completely depends on the measurement configuration. For instance, in the case of angular interrogation, the choice of the light source is always a monochromatic light, while for the wavelength interrogation, the choice will be polychromatic light at a fixed angle. The third type of configuration is phase interrogation, which requires a coherent monochromatic light source and extensive optical instrumentation for data acquisition. It has been reported that angular interrogation is more sensitive than wavelength-based interrogation, however, it involves moving optical parts. The requirement of the moving optical instrumentation limits the angular interrogation for the development of the point-of-care (PoC) sensor systems, nevertheless, a laboratory-based step up is

Figure 14. Illustrates the proposed machine learning (ML) approaches applied to surface plasmon resonance (SPR) sensorgrams. a) The block diagram outlines the tasks executed based on the responses of sensorgrams, encompassing describing, classifying, identifying, analyzing, and testing. b) The context of TSD (Time Series Descriptors) application is depicted, showcasing examples of sensorgram groups (a–d), TSD applied to a sensorgram with three permanent regimes e), coefficients plotting, and the labeling/classification of a new sensorgram as part of another element in group 12 (f). The accuracy of the k-NN algorithm for different distances is represented in (g). In (c), the figure provides a proof-of-concept for Leishmaniasis detection with positive (a) and negative (b) tests. Temporal and vertical differences do not impact classification. The detailed TSD application includes the indication of $\lambda \cdot r$ (mean resonance wavelength) for each substance by the red dot, linear regression parameters (β_1) for permanent (brown dots) and transition (black dots) regimes, regimes segmentation (c), and a hypothesis test to verify the presence of a substance in the experimental protocol (d). The confidence level defines the upper and lower limits of the confidence interval (CI), and the hypothesis test assesses if the regression coefficient is statistically zero within the established time window. The inset demonstrates, for instance, a time range (807–1040 s) where the confidence level = 99.9% could not confirm the presence of a substance, indicating a transition regime. Reproduced with permission from.^[89] Copyright 2020, Elsevier.

still a choice. The modern PoC-based GC-SPR systems exploit the display light or flashlights as a light source and cameras with charge-coupled devices (CCD) or CMOS (complementary metal-oxide-semiconductor) devices for wavelength interrogation. The developed systems also seem to provide reliable responses leading to a promising future with better smart sensing technologies. Such GC-SPR sensor systems could be used as a low-cost sensor platform for PoC diagnostics in resource-limited settings. Furthermore, the azimuthal rotation of the GC-SPR chip for enhanced sensitivity is being explored, which could result in the development of a sensitive analytical system with desired sensitivity for various applications. It is interesting to note that all these points hold true for conventional prism-based SPR. To increase the superiority over conventional SPR setups, GC-SPR has several advantages such as reducing the complexity of the sensor setup without the need for a prism. More importantly, the ergonomic design allows placing the light source and detector on the same side enabling ease in sensor design for instance smartphone integration.

As shown in this review, several applications have been demonstrated exploiting GC-SPR systems for the detection of various molecules not limited to proteins, nucleic acids, lipids, and small molecules. In simple words, irrespective of the analyte molecule the sensor performance completely depends on the effective refractive index change at the interface due to the biomolecular interaction, which in turn depends on the surface coverage. These facts bring in other features to be considered for developing GC-SPR systems, apart from the system configuration as discussed before. The surface coverage of analyte molecules depends on the surface chemistry, the bioreceptor immobilized on the sensor surface, the molecular weight of the analyte molecules, and their binding affinity. In addition, the major challenge is to confine the biomolecular interaction within the sensitive volume (evanescent field) of the surface plasmons. For instance, the use of short peptides and aptamers as ligands is known to confine the analyte interaction within the sensitive volume owing to their small size. In addition, these ligands offer better stability compared to antibodies, which are the most widely used. Commercial prism-based SPR systems are capable of detecting 1 pg mm^{-2} of adsorbed molecules, while such performance skill needs to be achieved for GC-SPR systems.

Overall GC-SPR systems hold significant potential for translation into practical applications, particularly in the realm of miniaturized and integrated lab-on-chip platforms and microfluidic devices. These compact systems are ideal for PoC diagnostics and portable healthcare solutions due to their ease of integration and potential for real-time, label-free sensing. Modern fabrication techniques enhance their attractiveness for large-scale production, ensuring cost-effectiveness and scalability. Moreover, the incorporation of machine learning (ML) and artificial intelligence (AI) tools can significantly improve the performance of GC-SPR devices, paving the way for Internet of Things (IoT)-based healthcare solutions. This advancement aligns well with the global medical sensor market, which was valued at \$15 billion in 2022 and is anticipated to grow at a compound annual growth rate (CAGR) of 10% until 2032. Despite these promising attributes, several challenges must be addressed for GC-SPR technology to achieve widespread clinical adoption. Sensitivity optimization remains a critical area, as further enhancements are required to match or

exceed the performance of existing diagnostic methods in specific applications. Additionally, establishing standardized protocols and benchmarks for GC-SPR-based diagnostics is essential to ensure consistency and reliability. Extensive clinical trials and validation studies will also be necessary to confirm the efficacy and reliability of GCSPR sensors for targeted medical applications, ultimately supporting their transition from the laboratory to routine clinical practice.

Acknowledgements

Open access funding enabled and organized by Projekt DEAL.

Conflict of Interest

The authors declare no conflict of interest.

Author Contributions

D.M. and M.T. contributed equally to this work.

Keywords

biosensor, chemical sensor, fabrication methods, GC-SPR, plasmonics, SPR

Received: August 2, 2024
Published online:

- [1] R. B. M. Schasfoort, A. J. Tudos, *Handbook of Surface Plasmon Resonance*, RSC Publishing, Cambridge, England **2008**.
- [2] L. Casemiro Oliveira, A. Marcus Nogueira Lima C. Thirstrup, H. Franz Neff, *Surface Plasmon Resonance Sensors*, 2nd ed. Springer, Berlin Heidelberg **2015**.
- [3] L. Bo, N. Claes, L. Ingemar, *Biosens. Bioelectron.* **1995**, *10*.
- [4] R. B. M. Schasfoort, *Handbook of Surface Plasmon Resonance*, 2nd ed. (Ed.: R. B. M. Schasfoort), The Royal Society of Chemistry **2017**, pp. 1–26, <https://doi.org/10.1039/9781788010283-00001>.
- [5] D. Shankaran, K. Gobi, N. Miura, *Sens. Actuators, B* **2007**, *121*, 158.
- [6] Y. Mo, Z. Pan, C. Xiang, L. Zhu, presented at 3rd International Academic Exchange Conference on Science and Technology Innovation, **2021**, pp. 1027–1031, <https://doi.org/10.1109/IAECST54258.2021.9695569>.
- [7] R. L. Rich, D. G. Myszyka, *Drug Discov Today Technol* **2004**, *1*, 301.
- [8] P. Singh, *Sens. Actuators, B* **2016**, *229*, 110.
- [9] M. F. S. Ferreira, G. Brambilla, L. Thevenaz, X. Feng, L. Zhang, M. Sumetsky, C. Jones, S. Pediredy, F. Vollmer, P. D. Dragic, O. Henderson-Sapir, D. J. Ottaway, E. Strupiechonski, G. G. Hernandez-Cardoso, A. I. Hernandez-Serrano, F. J. Gonzalez, E. Castro Camus, A. Mendez, P. Saccomandi, Q. Quan, Z. Xie, B. M. Reinhard, M. Diem, *J Opt* **2024**, *26*, 013001.
- [10] G. Guenter, *Anal. Bioanal. Chem.* **2005**, *381*, 141.
- [11] N. Sabri, S. A. Aljunid, M. S. Salim, R. B. Ahmad, R. Kamaruddin, *J. Phys.: Conf. Ser.* **2013**, *423*, 012064.
- [12] M. Li, S. K. Cushing, N. Wu, *Analyst* **2015**, *140*, 386.
- [13] H. Jiri, K. Ivo, Y. Sinclair S, *Sens. Actuators, B* **1999**, *54*, 16.
- [14] P. S. Vukusic, G. P. Bryan-Brown, J. R. Sambles, *Sens. Actuators, B* **1992**, *8*, 155.

- [15] M. Seo, J. Lee, M. Lee, *Opt. Express* **2017**, *25*, 26939.
- [16] G. P. Bryan-Brown, S. J. Elston, J. R. Sambles, *J Mod Opt* **1991**, *38*, 1181.
- [17] S. Rossi, E. Gazzola, P. Capaldo, G. Borile, F. Romanato, *Sensors (Basel)* **2018**, *18*, <https://doi.org/10.3390/s18051621>.
- [18] J. Dostálek, J. Homola, M. Miler, *Sens. Actuators, B* **2005**, *107*, 154.
- [19] T. Kan, K. Matsumoto, I. Shimoyama, *J. Micromech. Microeng.* **2010**, *20*, 085032.
- [20] J. Homola, in *Surface Plasmon Resonance Based Sensors*, Vol. 4, Springer-Verlag, Berlin Heidelberg, **2006**.
- [21] X. Dou, P. Y. Chung, P. Jiang, J. Dai, *Appl. Phys. Lett.* **2012**, *100*.
- [22] Y. Saito, S. Suzuki, T. Kan, *Appl. Phys. Express* **2021**, *14*, 036503.
- [23] K. Aliqab, R. Agravat, D. Agravat, S. K. Patel, M. Alsharari, A. Armghan, *Plasmonics* **2024**, <https://doi.org/10.1007/s11468-024-02336-y>.
- [24] A. Sonato, M. Agostini, G. Ruffato, E. Gazzola, D. Liuni, G. Greco, M. Travagliati, M. Cecchini, F. Romanato, *Lab Chip* **2016**, *16*, 1224.
- [25] G. Ruffato, E. Pasqualotto, A. Sonato, G. Zacco, D. Silvestri, M. Morigo, A. De Toni, F. Romanato, *Sens. Actuators, B* **2013**, *185*, 179.
- [26] G. Borile, S. Rossi, A. Filippi, E. Gazzola, P. Capaldo, C. Tregnago, M. Pigazzi, F. Romanato, *Biophys. Chem.* **2019**, *254*, 106262.
- [27] C. Sheng-Yu, L. Yung-Sung, C. Nai-Jen, Y. Jenq-Nan, M. Wen-Yi, C. Kuo-Chi, L. Chih-Ming, presented at 3rd International Conference on Nano/Molecular Medicine and Engineering, Taiwan **2009**.
- [28] E. Gazzola, A. Pozzato, G. Ruffato, E. Sovernigo, A. Sonato, *Optofluidics, Microfluidics and Nanofluidics* **2016**, *3*.
- [29] S. Long, J. Cao, Y. Wang, S. Gao, N. Xu, J. Gao, W. Wan, *Sens Actuators Rep* **2020**, *2*, 100016.
- [30] T. Keiko, H. Hironobu, K. Kenji, K. Kazuyuki, T. Yoshiro, N. Junji, *Opt. Express* **2008**, *16*, 9781.
- [31] K. Tawa, F. Kondo, C. Sasakawa, K. Nagae, Y. Nakamura, A. Nozaki, T. Kaya, *Anal. Chem.* **2015**, *87*, 3871.
- [32] J. Zhang, I. Khan, Q. Zhang, X. Liu, J. Dostalek, B. Liedberg, Y. Wang, *Biosens. Bioelectron.* **2018**, *99*, 312.
- [33] N. Zhang, H. Liu, W. Knoll, *Biosens. Bioelectron.* **2009**, *24*, 1783.
- [34] D. Yoo, A. Barik, F. de Leon-Perez, D. A. Mohr, M. Pelton, L. Martin-Moreno, S. H. Oh, *ACS Nano* **2021**, *15*, 6669.
- [35] Y. Wei-Hsun, K. Justin, H. Andrew C, *Anal. Chem.* **2010**, *82*, 4988.
- [36] J. S. Wi, S. Lee, S. H. Lee, D. K. Oh, K. T. Lee, I. Park, M. K. Kwak, J. G. Ok, *Nanoscale* **2017**, *9*, 1398.
- [37] Q. Wang, Y. Zheng, C. Yu, X. Chen, E. Wang, S. Long, H. Zhu, S. Gao, J. Cao, *Plasmonics* **2020**, *15*, 1639.
- [38] M. Vala, K. Chadt, M. Piliarik, J. Homola, *Sens. Actuators, B* **2010**, *148*, 544.
- [39] M. Vala, F. Baldini, J. Dostálek, J. Homola, presented at Proc. SPIE, 6585, Optical Sensing Technology and Applications, 658522, (16 May 2007), <https://doi.org/10.1117/12.723131>.
- [40] S. Long, J. Cao, S. Geng, N. Xu, W. Qian, S. Gao, *Opt. Commun.* **2020**, *476*, 126310.
- [41] W. Su, *Optik* **2017**, *131*, 104.
- [42] M. Bianco, A. Sonato, A. De Girolamo, M. Pascale, F. Romanato, R. Rinaldi, V. Arima, *Sens. Actuators, B* **2017**, *241*, 314.
- [43] A. Bijalwan, V. Rastogi, *Appl. Opt.* **2017**, *56*, 9606.
- [44] J. S. Yuk, E. F. Guignon, M. A. Lynes, *Chem. Phys. Lett.* **2014**, *591*, 5.
- [45] M. Tahmasebpour, M. Bahrami, A. Asgari, *Appl. Opt.* **2014**, *53*, 6307.
- [46] H. Hori, K. Tawa, K. Kintaka, J. Nishii, Y. Tatsu, *J. Appl. Phys.* **2010**, *107*, 114702.
- [47] J. P. Monteiro, L. B. Carneiro, M. M. Rahman, A. G. Brolo, M. J. L. Santos, J. Ferreira, E. M. Girotto, *Sens. Actuators, B* **2013**, *178*, 366.
- [48] J. Cao, Y. Sun, Y. Kong, W. Qian, *Sensors (Basel)* **2019**, *19*, 405.
- [49] V. Biswas, R. Vijaya, *Photonics and Nanostructures – Fundamentals and Applications* **2024**, *58*, 101199.
- [50] W. Hui, T. Chenghao, G. Xiaowan, L. Zhiqi, S. Jian, L. Chaoyang, *Photonics* **2023**, *10*, 899.
- [51] M. Abutoama, I. Abdulhalim, *Opt. Express* **2015**, *23*, 28667.
- [52] A. K. Sharma, A. K. Pandey, *J. Opt. Soc. Am. B* **2019**, *36*, F25.
- [53] X. Zhu, B. Wang, *Appl. Phys. Lett.* **2023**, *123*.
- [54] R. Hidayat, J. S. Pradana, A. Fariz, S. Komalasari, S. Chalimah, H. Bahar, *Sci. Rep.* **2023**, *13*, 5274.
- [55] X. Lu, P. Damborský, W. M. Munief, J. Ka-Yan Law, X. Chen, J. Katrlík, V. Pachauri, S. Ingebrandt, *Biosens Bioelectron X* **2022**, *11*, 100152.
- [56] X. Chen, M. Pan, K. Jiang, *Microelectron. Eng.* **2010**, *87*, 790.
- [57] Y. Wang, J. Dostalek, W. Knoll, *Anal. Chem.* **2011**, *83*, 6202.
- [58] Y. Wang, W. Knoll, J. Dostalek, *Anal. Chem.* **2012**, *84*, 8345.
- [59] D. Le, A. Ranta-Lassila, T. Sipola, M. Karppinen, J. Petäjä, M. Kehusmaa, S. Aikio, T. L. Guo, M. Roussey, J. Hiltunen, A. Popov, *Photonics Research* **2024**, *12*, 947.
- [60] E. Wang, J. Cao, K. Cao, N. Xu, H. Zhu, *Optical Engineering* **2023**, *62*, 017105.
- [61] S. Long, E. Wang, M. Wu, H. Zhu, N. Xu, Y. Wang, J. Cao, *Sens. Actuators, A* **2022**, *337*, 113416.
- [62] W. A. Challener, R. R. Ollmann, K. K. Kam, *Sens. Actuators, B* **1999**, *56*, 254.
- [63] F. Eduardo, *Appl. Opt.* **2004**, *43*, 79.
- [64] S. Mohapatra, U. Pant, R. S. Moirangthem, *Mater Today Proc* **2020**, *28*, 215.
- [65] C. Young-Ho, J. Young-Hyun, *E-J. Surf. Sci. Nanotechnol.* **2009**, *7*, 750.
- [66] B. Kaplan, H. Guner, O. Senlik, K. Gurel, M. Bayindir, A. Dana, *Plasmonics* **2009**, *4*, 237.
- [67] W. A. Murray, W. L. Barnes, *Adv. Mater.* **2007**, *19*, 3771.
- [68] Z. Fang, X. Zhu, *Adv. Mater.* **2013**, *25*, 3840.
- [69] W. Su, G. Zheng, X. Li, *Opt. Commun.* **2012**, *285*, 4603.
- [70] G. V. Naik, V. M. Shalaev, A. Boltasseva, *Adv. Mater.* **2013**, *25*, 3264.
- [71] S. Singh, S. Pandey, S. Yadav, R. K. Yadav, P. K. Singh, P. Lohia, D. K. Dwivedi, *J Opt* **2023**, *53*, 304.
- [72] D. Kumar, M. Khurana, M. Sharma, V. Singh, *Mater Today Proc* **2023**, <https://doi.org/10.1016/j.matpr.2023.02.319>.
- [73] M. W. Knight, N. S. King, L. Liu, H. O. Everitt, P. Nordlander, N. J. Halas, *ACS Nano* **2014**, *8*, 834.
- [74] W. Li, K. Ren, J. Zhou, *Trends Analyt Chem* **2016**, *80*, 486.
- [75] I. Z. Indutnyi, V. I. Mynko, M. V. Sopinsky, P. M. Lytvyn, V. A. Dan'ko, *Plasmonics* **2022**, *17*, 2459.
- [76] S. Ogawa, M. Iwakawa, M. Shimatani, S. Fukushima, *J. Appl. Phys.* **2024**, *135*.
- [77] E. R. Kim, C. Joe, R. J. Mitchell, M. B. Gu, *Trends Biotechnol.* **2023**, *41*, 374.
- [78] M. Divagar, R. Bandaru, V. Janakiraman, V. V. R. Sai, *Biosens. Bioelectron.* **2020**, *167*, 112488.
- [79] M. Divagar, R. Gayathri, R. Rasool, J. K. Shamee, H. Bhatia, J. Satija, V. V. R. Sai, *IEEE Sens. J.* **2021**, *21*, 22758.
- [80] P. Lisboa, A. Valsesia, I. Mannelli, S. Mornet, P. Colpo, F. Rossi, *Adv. Mater.* **2008**, *20*, 2352.
- [81] *Kuby Immunology*, (Eds.: S. A. Stranford, J. A. Owen, J. Punt, P. Jones), 8th ed., Macmillan Education, New York **2019**.
- [82] S. Ahmed, J. Ning, D. Peng, T. Chen, I. Ahmad, A. Ali, Z. Lei, M. Abu Bakr Shabbir, G. Cheng, Z. Yuan, *Food Agric. Immunol.* **2020**, *31*, 268.
- [83] S. Kirby M, G. Saad J, *Lab Med* **1996**, *27*.
- [84] C. Davies, in *The Immunoassay Handbook*, (Ed: D. Chris), Elsevier Ltd, Amsterdam, Netherlands **2013**.
- [85] D. Kotlarek, M. Vorobii, W. Ogieglo, W. Knoll, C. Rodriguez-Emmenegger, J. Dostalek, *ACS Sens.* **2019**, *4*, 2109.
- [86] J. Zhou, M. R. Battig, Y. Wang, *Anal. Bioanal. Chem.* **2010**, *398*, 2471.
- [87] D. Le, A. Ranta-Lassila, T. Sipola, M. Karppinen, J. Petäjä, M. Kehusmaa, S. Aikio, T.-I. Guo, M. Roussey, J. Hiltunen, A. Popov,

- Presented at Proc. SPIE 12991, Nanophotonics X, (10 June 2024), 129910E, <https://doi.org/10.1117/12.3017505>.
- [88] Y. Dogan, R. Katirci, İ. Erdogan, E. Yartasi, *Opt. Commun.* **2023**, 534, 129332.
- [89] J. C. M. Gomes, L. C. Souza, L. C. Oliveira, *Biosens. Bioelectron.* **2021**, 172, 112760.
- [90] K. Rastogi, A. K. Sharma, Y. K. Prajapati, *Appl. Phys. A* **2023**, 129, 351.
- [91] J. Zheng, Z. C. Ye, C. L. Wang, Y. F. Fu, X. R. Huang, Z. M. Sheng, *Adv. Mater. Technol.* **2019**, 4, <https://doi.org/10.1002/admt.201800661>.
- [92] S. Aksu, M. Huang, A. Artar, A. A. Yanik, S. Selvarasah, M. R. Dokmeci, H. Altug, *Adv. Mater.* **2011**, 23, 4422.
- [93] A. Rodriguez, M. Echeverría, M. Ellman, N. Perez, Y. K. Verevkin, C. S. Peng, T. Berthou, Z. Wang, I. Ayerdi, J. Savall, S. M. Olaizola, *Microelectron. Eng.* **2009**, 86, 937.
- [94] M. Weidong, W. Ishan, C. Chang-Hwan, *Optics Letter* **2011**, 36, 3176.
- [95] M. Huang, Y. Cheng, F. Zhao, Z. Xu, *Ann. Phys.* **2012**, 525, 74.
- [96] I. A. Sassi, M. B. El Hadj Rhouma, M. G. Daher, *Opt Quantum Electron* **2023**, 55, <https://doi.org/10.1007/s11082-023-04682-3>.
- [97] A. K. Pandey, H. Kumar, *Opt Quantum Electron* **2022**, 55, <https://doi.org/10.1007/s11082-022-04327-x>.
- [98] A. Armghan, B. B. Han, D. Agravat, K. Alqiab, M. Alsharari, S. K. Patel, *Plasmonics* **2024**, <https://doi.org/10.1007/s11468-024-02369-3>.
- [99] M. Alsharari, J. Wekalao, S. K. Patel, A. K. U., K. Aliqab, A. Armghan, *Plasmonics* **2024**, <https://doi.org/10.1007/s11468-024-02372-8>.



Divagar Murugan received a B.Sc. degree in Biotechnology from SRM University, Chennai in 2014 and an M.Sc. degree (2014-2016) in Nanoscience and Nanotechnology from the University of Madras, Chennai, in 2016. Later, he pursued a Ph.D. degree (2017-2022) in plasmonic fiberoptic absorbance biosensors at the Indian Institute of Technology Madras (IITM) under the Innovation in Science Pursuit for Inspired Research (INSPIRE) Research Fellowship from the Department of Science and Technology, Government of India (DST-India). Currently, he is working as a Post-doctoral researcher in the Interfaces of Bio-Nanosystems research group at the Institute of Materials in Electrical Engineering 1 (IWE1), RWTH Aachen University, Germany. His current research focuses on the development of integrated solutions for clinical diagnostics, using advanced plasmonics, material interface, surface engineering, and machine learning techniques.



Marcel Tintelott received the B.Sc. and M.Sc. degrees in electrical engineering from the University of Bremen, Germany, in 2017 and 2018. In 2018, he joined the Micro- and Nanoelectronic Sensors Group of the Institute of Materials in Electrical Engineering 1. His research includes the fabrication of field-effect-based biosensors and their use in novel nucleic acid detection principles for increased sensor performance. In 2023, he obtained his Dr. Ing degree in the faculty of Electrical Engineering and Information Technology of RWTH Aachen University, Germany. His current research focuses on biosensors and its technology.



Narayanan Madaboosi is currently a DBT-Ramalingaswami Re-Entry Faculty at IIT Madras, India. He holds a Ph.D. in Biotechnology, with a background in Healthcare Engineering, in general and point-of-care diagnostics, in particular. His expertise includes biosensors, microfluidics, bioassays, and readout platforms for infectious diseases and cancers. He has worked on several EU projects, spanning international academic, industry, and innovation ecosystem backgrounds.



Xuan-Thang Vu studied his master in material science at Hanoi University of Science and Technology (HUST), Vietnam, and worked as a staff scientist at the International Training Institute for Materials Science (ITIMS), HUST, Vietnam from 2003 to 2006. In 2006, he started doctoral studies at the Research Center Jülich in the Institute of Bio- and Nanosystems (IBN), Institute 2 Bioelectronics working on the topic of top-down fabrication of silicon nanowire transistor arrays for biosensor applications. From 2010 to 2013, he worked as a postdoctoral scientist at the University of Applied Sciences Kaiserslautern in the Biomedical Signalling group for the development of micro- and nanoelectronic sensors for biomedical applications. From 2014 to 2018, he was a postdoctoral scientist at RWTH Aachen University in the Dynamics of Amorphous Semiconductors research group at the 1st Institute of Physics (IA), Physics of New Materials working on nanoscale devices enabling detailed investigations of phase change materials using simultaneous electrical and in situ/operando TEM characterization. 2021 onward, he is a research group leader of the Micro- and Nanoelectronic Sensors at IWE 1, RWTH Aachen.



Tetiana Kurkina holds a Master's degree from Taras Shevchenko National University (Kyiv, Ukraine). Her academic journey led her to the Max Planck Institute for Solid State Research (Stuttgart, Germany), where she completed her Ph.D. thesis on carbon material-based biosensors, earning a Dr.rer.nat. in Chemistry from Justus Liebig University Giessen in 2012. Post-Ph.D., Tetiana broadened her expertise through roles in a collaborative lab (Carbon Materials Innovation Center) between BASF SE and the Max Planck Institute for Polymer Research at BASF headquarters in Ludwigshafen, followed by a position at the Technical University of Kaiserslautern. Since November 2018, Dr. Tetiana Kurkina has been an integral part of RWTH Aachen, Chair of Biotechnology (under the guidance of Prof. Schwaneberg). In her versatile role, she spearheads projects in protein engineering for applications in agriculture, the food industry, and biosensors. Her commitment to advancing biotechnological solutions reflects her dedication to transformative research and innovation, contributing significantly to the field.



César Rodríguez-Emmenegger studied Chemical Engineer at Universidad de la República, Uruguay; and a PhD in Biophysics and Macromolecular Chemistry and Physics at the Institute of Macromolecular Chemistry in Prague under the mentorship of Eduard Brynda and Aldo Bologna Alles. Presently, he is a Research Professor at the Institute for Bioengineering of Catalonia (IBEC) and the Catalan Institute for Research and Advanced Studies (ICREA) in Barcelona, Spain, and an Associate Scientist at DWI-Leibniz Institute for Interactive Materials in Aachen. The overarching goal of his research is to uncover design rules to develop materials capable of communicating with living matter—pathogens, cells, tissues—and directing its behavior in a self-regulated manner to enable new biomaterials, therapeutics, and medical devices. He



Ulrich Schwaneberg graduated in chemistry (in 1996) and received his PhD (in 1999; supervisor Prof. R. D. Schmid) from the University in Stuttgart. He was, after a post-doc at Caltech in the lab of the Nobel laureate Prof. Frances H. Arnold, appointed as Professor at the Jacobs University Bremen in 2002. In January 2009, he moved to the RWTH Aachen University as Head of the Institute of Biotechnology and since 2010 co-appointed in the Scientific Board of Directors at the DWI Leibniz Institute for Interactive Materials. Furthermore, he coordinates with Prof. Bergs the competence center Bio4MatPro (one of two BMBF flagship projects in the bioeconomy model region), serves on the board of directors in the Bioeconomy Science Center, and is Speaker of the RWTH profile area Molecular Science & Engineering. He is a co-founder of the companies SeSaM Biotech & Aachen Proteineers and has a special interest in Protein engineering to provide tailored proteins and hybrid catalysts as building blocks for the biological transformation of material science and sustainable recycling processes. In 2016, he received the BMBF-Forschungspreis for the next generation of bioprocesses, has published >370 original manuscripts, and is a coinventor on >30 patents, mostly with industry.



Jakub Dostalek studied optics and optoelectronics (1995–2000) and received his Ph.D. (2006) in Quantum Optics and Optoelectronics, focusing on surface plasmons. Following his post-doctoral experience at Max Planck Institute for Polymer Research, Mainz, Germany, and research stays as a visiting scientist and senior scientist at Nanyang Technology University, Singapore, Institute of Physics, Czech Academy of Sciences, Prague, Czech Republic, AIT-Austrian Institute of Technology GmbH, Vienna, Austria. He is currently working as a Lecturer, at Technikum Wien FH, Vienna, Austria, University of Natural Resources and Life Sciences, Institute of Biophysics, Vienna, Austria, Senior Scientist at Danube Private University, Tulln, Austria, and the Institute of Physics, Czech Academy of Sciences, Prague, Czech Republic.



Sven Ingebrandt received his degree in Physics in 1998 and a doctoral degree in Physical Chemistry in 2001, both awarded by the Johannes-Gutenberg-University Mainz, Germany. During his doctorate, he worked at the Max-Planck Institute for Polymer Research Mainz, Germany. Afterward he joined from 2001 to 2002 the Frontier Research Program at RIKEN Institute, Tokyo, Japan, as a post-doctoral researcher. In 2002, he was a group leader in the Institute of Bio- and Nanosystems at the Forschungszentrum Jülich GmbH, Germany. From 2008 to 2017 he was appointed as a full professor of Biomedical Instrumentation at the University of Applied Sciences Kaiserslautern, Germany. In 2018, he moved to RWTH Aachen University as a professor of Micro- and Nanosystems and as the director of the Institute for Materials in Electrical Engineering 1 (IWE1). He is working at the interface between biotechnology, cell biology, nanotechnology, microelectronics, material science, and micro- and nanosystem technology. His main interests are micro- and nanochip design and fabrication, bioelectronic signal recording and interpretation, and neuronal implants with an emphasis on nanoscale ion-sensitive field-effect transistors, electrochemical impedance spectroscopy techniques, organic transistors, and optoelectronic devices.



Vivek Pachauri is the research group leader of Interfaces of BioNano-systems at the Institute of Materials in Electrical Engineering 1 (IWE1) at RWTH Aachen University. He studied biology and chemistry as an undergraduate and developed an interest in implementing soft-chemistry approaches for the realization of nanoelectronic, optical devices for sensor and biosensor applications. He received a doctoral degree in Physics from the Ecole Polytechnique Federale de Lausanne (EPFL), Switzerland in 2011. As a postdoctoral fellow at the Max Planck Institute for Solid State Research Stuttgart, he furthered his work on novel device concepts for sensing in liquids using low-dimensional semiconductors electrical and optical transducers. He took a leading research role in establishing cleanroom-based nanofabrication processes for top-down integration of graphene and silicon-based biosensors at the Biomedical Signalling Group at the University of Applied Sciences Kaiserslautern. Current activities in his research group aim toward the development of bio-inspired interfaces and systems for sustainable development of clinical use biosensor platforms and biohybrid computation strategies.